Mon. Not. R. Astron. Soc. **000**, 000–000 (0000) Printed 2 February 2008 (MN LATEX style file v2.2)

Theory and practice of microlensing lightcurves around fold singularities

M. Dominik
University of St Andrews, School of Physics & Astronomy, North Haugh, St Andrews, KY16 9SS, United Kingdom

2 February 2008

ABSTRACT

Among all galactic microlensing events, those involving a passage of the observed source star over the caustic created by a binary lens are particularly useful in providing information about stellar atmospheres, the dynamics of stellar populations in our own and neighbouring galaxies, and the statistical properties of stellar and sub-stellar binaries. This paper presents a comprehensive guide for modelling and interpreting the lightcurves obtained in events involving fold-caustic passages. A new general, consistent, and optimal choice of parameters provides a deep understanding of the involved features, avoids numerical difficulties and minimizes correlations between model parameters. While the photometric data of a microlensing event around a caustic passage itself do not provide constraints on the characteristics of the underlying binary lens and do not allow predictions of the behaviour of other regions of the lightcurve, vital constraints can be obtained in an efficient way if these are combined with a few simple characteristics of data outside the caustic passages. A corresponding algorithm containing some improvements over an earlier approach which takes into account multi-site observations is presented and discussed in detail together with the arising parameter constraints paying special attention to the role of source and background fluxes.

Key words: gravitational lensing – methods: data analysis – stars: atmospheres – binaries: general – stars: low-mass, brown dwarfs – Galaxy: stellar content.

1 INTRODUCTION

The majority of the galactic microlensing events that have been detected or are currently detected are compatible with both the observed source star and the compact massive lens being approximated by point-like objects. However, about 2 to 3 per cent of the events involve peaks lasting from a few hours to a few days whose shape is characteristic for the source crossing a fold-caustic line which is created by a binary (or multiple) lens object. These fold-caustic passage events provide valuable information about both the source star and the lens object not being extractable from 'ordinary' microlensing events.

Microlensing events compatible with a point-like source at distance $D_{\rm S}$ and a point-like lens of mass M at distance $D_{\rm L}$ involve only one parameter that is related to physical properties of lens or source and carries a dimension, namely the time-scale of motion $t_{\rm E} = \theta_{\rm E}/\mu$, where μ denotes the proper motion of the source relative to the lens and $\theta_{\rm E}$ is the angular Einstein radius, given by

$$\theta_{\rm E} = \sqrt{\frac{4GM}{c^2}\,\frac{D_{\rm S}-D_{\rm L}}{D_{\rm S}\,D_{\rm L}}}\,. \qquad (1)$$

The time-scale of motion $t_{\rm E}$ is therefore a convolution of the lens mass M, the lens distance $D_{\rm L}$, and the proper motion μ, which cannot be measured individually, so that the power of ordinary microlensing events for the determination of the mass function and phase-space distribution of stellar populations in our own or neighbouring galaxies that have caused these events is severely limited (Mao & Paczynski 1996). In contrast to this, the observed duration of a fold-caustic passage $t_\star^\perp$ provides a second time-scale which is related to the angular size of the source star $\theta_\star$. An estimate for $\theta_\star$ can be obtained from the stellar flux and spectral type, so that $t_\star^\perp$ provides a lower limit to the proper motion μ by yielding its component $\mu^\perp = \theta_\star/t_\star^\perp$ perpendicular to the caustic, and $\mu = \mu^\perp/(\sin\phi)$ itself follows with a determination of the crossing angle ϕ from modelling the full observed lightcurve. The measurement of the relative proper motion between lens and source for a microlensing event toward the Small Magellanic Cloud (SMC) (Afonso et al. 1998; Albrow et al. 1999c,b; Afonso et al. 2000; Alcock et al. 1999; Rhie et al. 1999; Udalski et al. 1998) indicated that the lens in located in the SMC rather than in the Galaxy, giving support to the hypothesis that the majority of microlensing events toward the SMC are due to self-lensing among its stellar populations (e.g. Di Stefano 2000).

In addition to providing a measurement of the proper motion μ, lightcurves around caustic passages are particularly sensitive to effects caused by the parallactic motion of the Earth around the Sun or by the orbital motion of the binary lens (Hardy & Walker 1995; Gould & Andronov 1999). Observations of these effects and the determination of the corresponding parameters (e.g. Dominik 1998)

together with the determination of the proper motion μ break the degeneracy between the lens mass M and its distance $D_{\rm L}$ yielding measurements of the individual quantities (up to possible discrete ambiguities). One such measurement has been reported by An et al. (2002).

The characteristic and distinctive shape of the lightcurve around caustic passages allows to obtain stronger constraints on the parameters of the binary lens than those resulting from binary lens events that show only weak deviations compared to single lenses. Therefore fold-caustic passage events provide the main source of information about the statistical distributions of the properties of stellar and sub-stellar binaries such as the total mass, mass ratio, semimajor axis, or orbital period.

The most valuable results arising from caustic-passage microlensing events so far have been on the study of stellar atmospheres. The strong differential magnification that arises as the source passes over the caustic allows to resolve surfaces of source stars at Galactic distances providing a powerful and unique technique to study stellar atmospheres of a variety of different types of stars thereby probing existing theoretical models (Schneider & Weiß 1987; Rhie & Bennett 1999; Gaudi & Gould 1999). Measurements of limb-darkening coefficients from binary lens microlensing events have been published for three K-giants (Albrow et al. 1999a, 2000; Fields et al. 2003), one G/K-subgiant (Albrow et al. 2001a) and a Solar-like star (Abe et al. 2003) in the Galactic bulge as well as for an A-dwarf in the SMC (Afonso et al. 2000), where the source sweeps over a cusp for two of these events. In addition to a dense photometric coverage during the course of a caustic passage, the observation of a temporal sequence of spectra provides a probe of the spatial distribution of chemical elements (Gaudi & Gould 1999) using the observed variation of related spectral lines as indicators. For a galactic bulge microlensing event in 2000, several low-resolution spectra have been taken with the FORS1 spectrograph at the VLT (ESO Paranal, Chile) showing a significant variation of the equivalent width of the Hα-line by Albrow et al. (2001b), while two high-resolution spectra have been taken at the Keck telescope (Mauna Kea, Hawaii, USA) by Castro et al. (2001), and both measurements have later been discussed by Afonso et al. (2001). In 2002, a dense sequence of high-resolution spectra has been obtained for another event with the UVES spectrograph at the VLT where significant equivalent-width variations in the most prominent lines Hα, Hβ, and Ca II have been detected (Cassan et al. 2004; Beaulieu et al. 2004).

In addition to the events already discussed in the literature, a dense high-precision photometric coverage of caustic-passage regions of several further microlensing events allowing the determination of limb-darkening coefficients has been obtained by PLANET[1] (Albrow et al. 1998; Dominik et al. 2002) during recent years, and additional data on caustic-passage events have also been collected by other microlensing collaborations, namely EROS[2] (Afonso et al. 2003), MACHO[3] (Alcock et al. 2000a,b,c), OGLE[4] (Udalski, Kubiak & Szymański 1997; Wozniak et al., 2001), MOA[5] (Sumi et al. 2003), MPS[6] (Rhie et al. 1999), and MicroFUN[7] (Yoo et al. 2004). With currently $\sim$500 microlensing alerts per year issued by OGLE-III[8] and $\sim$60 alerts per year issued by MOA[9], about 10–15 caustic-passage events per year can be expected for which limb-darkening coefficients of the source star can be obtained by a dense high-precision photometric coverage, while, depending on allocated resources, spectroscopic measurements should be feasible for a few events per year.

The aim of this paper is to provide a comprehensive guide for modelling and interpreting microlensing lightcurves near fold singularities which are produced by extended sources and binary lenses, and for finding all suitable models for microlensing events involving fold-caustic passages. In addition, the derivation of physical properties of the lens and the source resulting from the modelling of such events is discussed. This paper outlines the underlying theory and sets the notation for upcoming analyses of observed data. A similar paper about cusp singularities including a comparison with the relations for folds as discussed in this paper is under preparation.

For lightcurves near a fold-caustic passage, a new consistent, general, and optimal set of parameters which are directly related to observable features of the observed lightcurve is introduced. This choice not only leads to a better understanding of the features of the lightcurve by allowing an obvious interpretation in terms of corresponding properties of lens or source, but also minimizes correlations between the parameters. In addition, singularities in parameter space likely to cause numerical problems, e.g. when the source size tends to zero or the background flux assumes some special values (in particular for flux values arising from image-subtraction), are avoided.

Finding all suitable model parameters corresponding to lightcurves consistent with the observed data of a complex microlensing event is a non-trivial task due to the large number of parameters and intrinsic degeneracies and ambiguities between the physical properties of the source and the lens system (Mao & Di Stefano 1995; Dominik & Hirshfeld 1996; Di Stefano & Perna 1997; Dominik 1999a,b; Albrow et al. 1999b). Since the lightcurve of sources in the vicinity of the fold is determined by local properties related to the fold singularity, limb-darkening measurements do not require the assessment of models for the complete lightcurve along with arising ambiguities and degeneracies. However, a model of the full lightcurve is needed for determining the proper motion μ, the time-scale of motion $t_{\rm E}$ that carries information about lens mass M and distance $D_{\rm L}$, and the mass ratio q and the separation parameter $d = \delta/\theta_{\rm E}$ of the binary lens (where δ is the instantaneous angular separation between its components). Moreover, a dense coverage of the lightcurve during the caustic passage and in particular target-of-opportunity observations of spectra yielding a powerful test of the atmosphere of the source star require some prior arrangements pushing the need for a prediction of caustic passages. With the lightcurve near a caustic passage being determined by local properties only, a prediction is possible with data taken on the rise to a caustic exit, while the data taken over previous caustic passages itself do not provide any information, whereas the combination with previous data outside

[1] http://planet.iap.fr
[2] http://eros.in2p3.fr
[3] http://wwwMACHO.mcmaster.ca
[4] http://www.astrouw.edu.pl/~ftp/ogle
[5] http://www3.vuw.ac.nz/scps/moa
[6] http://bustard.phys.nd.edu/MPS
[7] http://www-astronomy.mps.ohio-state.edu/~microfun
[8] http://sirius.astrouw.edu.pl/~ogle/ogle3/ews/ews.html
[9] http://www.roe.ac.uk/~iab/alert/alert.html

caustic passages can yield some constraints (Albrow et al. 1999b; Jaroszyński & Mao 2001).

In general, the correlations between model parameters are minimized by choosing parameters that correspond to observable characteristics of the observed lightcurve. For binary lens caustic-passage microlensing events, the caustic passages themselves show some characteristic features. Restricting the full parameter space by modelling a caustic passage and performing a search in the lower-dimensional subspace holding additional parameters necessary to describe the full lightcurve therefore constitutes an efficient method for modelling such events (Albrow et al. 1999b). In this paper, an improved variant of this approach taking into account multi-site and/or multi-band observations is described and discussed in detail, and the relations between the fold-caustic model parameters, the properties of the binary lens, and observable characteristics of the full lightcurve such as the time-scale of motion or the source and background fluxes are investigated.

In Sect. 2, the basic theory of gravitational lensing is reviewed setting the basic notation used in this paper, while Sect. 3 gives a detailed discussion of the fold singularity and its properties. Sect. 4 investigates the magnification of source stars in the vicinity of fold caustics and Sect. 5 discusses the specific implications arising from limb darkening. Sect. 6 deals with lightcurves of source stars in a region close to a caustic passage within a microlensing event and presents an adequate parametrization of such parts of lightcurves to be used for modelling observed data where the model parameters directly correspond to observable properties of the lightcurve and can be easily understood. The determination of a complete set of parameters characterizing the full lightcurve by making use of the parameters locally characterizing the caustic region forms the content of Sect. 7, where two versions of the basic algorithm (differing in the consideration of the temporal variation of the magnification of non-critical images) are discussed, followed by discussions of constraints arising from non-negative background flux and from simple characteristics of the data outside the caustic-passage region such as the baseline flux or the time-scale of motion. In Sect. 8, the predictive power of the data in the caustic passage region and its combination with characteristics of data outside it with respect to the determination of the characteristics of the binary lens and the perspective for predicting future caustic passages is discussed. Sect. 9 finally provides a summary of the paper and its results. A table of the used symbols has been attached at the end of the paper.

2 THE LENS MAPPING

Gravitational lensing is understood as the bending of light emitted by a source caused by the gravitational field of intervening matter. Due to this effect, a source located at a position $\boldsymbol{y}$ on the sky (in arbitrarily scaled coordinates) will be observed at one or more image positions $\boldsymbol{x}^{(i)}$. Moreover, the luminosity of the observed images differs from the intrinsic luminosity of the source object. In general, a lens mapping can be described by the Fermat-Potential

$$\Phi(\boldsymbol{x},\boldsymbol{y}) = \frac{1}{2}\left(\boldsymbol{x}-\boldsymbol{y}\right)^2 - \psi(\boldsymbol{x}) \tag{2}$$

(Schneider 1985) corresponding to the arrival time of (hypothetical) light rays at the observer. Fermat's principle determines the actual light rays to satisfy

$$\boldsymbol{\nabla}_{\boldsymbol{x}}\Phi = 0\,, \tag{3}$$

which relates source and image positions by the lens equation

$$\boldsymbol{y} = \boldsymbol{x} - \boldsymbol{\alpha}(\boldsymbol{x})\,, \tag{4}$$

where

$$\boldsymbol{\alpha}(\boldsymbol{x}) = \boldsymbol{\nabla}_{\boldsymbol{x}}\psi(\boldsymbol{x})\,. \tag{5}$$

Let indices to Φ denote its n-th partial derivatives with respect to $x_{i_1}\ldots x_{i_n}$, i_k being the coordinate index of the k-th derivative, i.e.

$$\Phi_{i_1,\ldots,i_n} = \frac{\partial}{\partial x_{i_n}}\cdots\frac{\partial}{\partial x_{i_1}}\,\Phi\,, \tag{6}$$

and let $\psi_{i_1,\ldots,i_n}$ denote the corresponding derivatives of ψ. For (locally) continuous derivatives, the order of derivation and therefore the order of indices to Φ or ψ is irrelevant (Schwarz's theorem). For the second derivatives of Φ, one obtains the relation

$$\Phi_{ij}(\boldsymbol{x}) = \delta_{ij} - \psi_{ij}(\boldsymbol{x}) = \frac{\partial y_i}{\partial x_j}\,, \tag{7}$$

where δ_{ij} denotes the Kronecker symbol

$$\delta_{ij} = \begin{cases} 0 & \text{for} \quad i \neq j \\ 1 & \text{for} \quad i = j \end{cases}\,. \tag{8}$$

Eq. (7) implies that all derivates of $\boldsymbol{y}$ with respect to x_{i_k} can be expressed by means of the Fermat potential Φ and its derivatives. In particular, the components of the Jacobian matrix $\mathbf{J}$ read

$$\mathsf{J}_{ij} = \frac{\partial y_i}{\partial x_j} = \Phi_{ij}\,, \tag{9}$$

and its determinant becomes

$$\det\mathbf{J} = \Phi_{11}\,\Phi_{22} - \left(\Phi_{12}\right)^2. \tag{10}$$

The Jacobian determinant yields the (signed) magnification of an image at $\boldsymbol{x}^{(i)}$ as

$$\mu(\boldsymbol{x}^{(i)}) = \frac{1}{\det\mathbf{J}(\boldsymbol{x}^{(i)})}\,, \tag{11}$$

and the total magnification A of a source at $\boldsymbol{y}$ is obtained by summing over the absolute values of the individual magnifications of its N images, i.e.

$$A(\boldsymbol{y}) = \sum_{i=1}^{N}\left|\mu(\boldsymbol{x}^{(i)})\right|, \tag{12}$$

where $\boldsymbol{x}^{(i)}$ and $\boldsymbol{y}$ satisfy the lens equation.

The lens mapping becomes singular at points $\boldsymbol{x}^{(\mathrm{crit})}$ in image space for which the Jacobian determinant vanishes ($\det\mathbf{J}(\boldsymbol{x}^{(\mathrm{crit})}) = 0$) which themselves are called critical points. The set of critical points forms critical curves which are mapped onto the caustics by the lens equation. The number of images associated with a given source position changes (by multiples of two) with the source position if and only if the source crosses a caustic. Therefore, the caustics divide the two-dimensional space of source positions into regions with a fixed number of images, where a source is defined to be 'inside' a caustic if it belongs to the region with the larger number of images, and 'outside' the caustic otherwise. The singularities of the lens mapping can be categorized into different types showing their own specific characteristics.

3 THE FOLD SINGULARITY

The lowest-order singularity is the fold, for which the following conditions need to be fulfilled (Schneider & Weiß 1992):

- exactly one of the eigenvalues of the Jacobian matrix is zero,

- the tangent vector of the critical curve is not an eigenvector of the Jacobian matrix belonging to eigenvalue zero.

For critical points, the eigenvalues of **J** are given by

$$\lambda^{(1)} = \Phi_{11} + \Phi_{22} = \mathrm{Tr}\,\mathbf{J}\,, \quad \lambda^{(2)} = 0\,. \tag{13}$$

The first condition for a fold then implies that $\Phi_{11} + \Phi_{22} \neq 0$. Normalized eigenvectors that correspond to these eigenvalues can be written in the form

$$\boldsymbol{e}^{(1)} = \begin{pmatrix} \cos\theta \\ \sin\theta \end{pmatrix}\,, \quad \boldsymbol{e}^{(2)} = \begin{pmatrix} -\sin\theta \\ \cos\theta \end{pmatrix}\,, \tag{14}$$

where

$$\begin{aligned} \sin\theta &= \varepsilon(\Phi_{12}\,\Phi_{22})\,\sqrt{\left|\frac{\Phi_{22}}{\Phi_{11}+\Phi_{22}}\right|}\,, \\ \cos\theta &= \sqrt{\left|\frac{\Phi_{11}}{\Phi_{11}+\Phi_{22}}\right|}\,, \end{aligned} \tag{15}$$

with

$$\varepsilon(z) = \begin{cases} 1 & \text{for} \quad z \geqslant 0 \\ -1 & \text{for} \quad z < 0 \end{cases}\,. \tag{16}$$

The vanishing of the Jacobian determinant yields $\Phi_{11}\Phi_{22} = (\Phi_{12})^2 \geqslant 0$, so that $|\Phi_{11} + \Phi_{22}| = |\Phi_{11}| + |\Phi_{22}|$.

Let $\boldsymbol{x}_\mathrm{f}$ denote a point on the critical curve and $\boldsymbol{y}_\mathrm{f} = \boldsymbol{x}_\mathrm{f} - \boldsymbol{\alpha}(\boldsymbol{x}_\mathrm{f})$ denote the corresponding source coordinate on the fold caustic. The eigenvectors of **J** given by Eq. (14) then constitute a right-handed basis of a coordinate system defined by

$$\begin{aligned} \boldsymbol{x}(t) &= \boldsymbol{x}_\mathrm{f} + \boldsymbol{\mathcal{R}}\,\boldsymbol{x}'(t)\,, & (17) \\ \boldsymbol{y}(t) &= \boldsymbol{y}_\mathrm{f} + \boldsymbol{\mathcal{R}}\,\boldsymbol{y}'(t)\,, & (18) \end{aligned}$$

where

$$\boldsymbol{\mathcal{R}} = \begin{pmatrix} \cos\theta & -\sin\theta \\ \sin\theta & \cos\theta \end{pmatrix}\,, \tag{19}$$

so that θ is the orientation of the (x_1', x_2')- and (y_1', y_2')- coordinates with respect to the (x_1, x_2)- and (y_1, y_2)-coordinates, respectively. Since every multiple of an eigenvector is an eigenvector itself, $-(\boldsymbol{e}^{(1)}, \boldsymbol{e}^{(2)})$ also constitutes a right-handed basis being related to $(\boldsymbol{e}^{(1)}, \boldsymbol{e}^{(2)})$ by a 180°-rotation, equivalent to replacing θ by $\pi + \theta$. Eq. (17) implies that

$$\mathcal{R}_{ij} = \frac{\partial x_i}{\partial x_j'}\,. \tag{20}$$

The Jacobian matrices $\mathbf{J}(x_1, x_2)$ and $\mathbf{J'}(x_1', x_2')$, where $\mathsf{J}_{ij} = \partial y_i/\partial x_j$ and $\mathsf{J}'_{ij} = \partial y_i'/\partial x_j'$, are related by

$$\mathbf{J'} = \boldsymbol{\mathcal{R}}^\mathrm{T}\,\mathbf{J}\,\boldsymbol{\mathcal{R}}\,, \tag{21}$$

so that **J'** becomes diagonal. In analogy to Eq. (6), let indices to Φ' denote derivatives with respect to x_i'. The invariance of trace and determinant under the transformation given by Eq. (21) yields

$$\Phi'_{11} = \lambda^{(1)} = \Phi_{11} + \Phi_{22}\,, \quad \Phi'_{22} = \lambda^{(2)} = 0\,. \tag{22}$$

In the chosen coordinates, the gradient of the Jacobian determinant reads

$$\boldsymbol{\nabla}_{\boldsymbol{x}}\det\mathbf{J}' = \Phi'_{11}\,\begin{pmatrix} \Phi'_{122} \\ \Phi'_{222} \end{pmatrix}\,, \tag{23}$$

so that a tangent vector to the critical curve has to be proportional to $(-\Phi'_{222}, \Phi'_{122})^\mathrm{T}$. Therefore, the conditions for a fold become (Schneider & Weiß 1992)

- $\Phi'_{11} \neq 0$, $\Phi'_{22} = 0$,
- $\Phi'_{222} \neq 0$,

which guarantee that the gradient of the Jacobian determinant does not vanish. Taking into account these conditions and the specific choice of coordinates, the lens equation near a fold can be expanded as (Schneider et al. 1992, p. 183f.)

$$\begin{aligned} y_1' &= \Phi'_{11}x_1' + \frac{1}{2}\,\Phi'_{122}(x_2')^2 + \Phi'_{112}x_1'x_2'\,, & (24) \\ y_2' &= \frac{1}{2}\,\Phi'_{112}(x_1')^2 + \Phi'_{122}x_1'x_2' + \frac{1}{2}\,\Phi'_{222}(x_2')^2\,. & (25) \end{aligned}$$

Using this expansion, the Jacobian matrix near the fold reads

$$\mathbf{J}' = \begin{pmatrix} \Phi'_{11} + \Phi'_{112}x_2' & \Phi'_{112}x_1' + \Phi'_{122}x_2' \\ \Phi'_{112}x_1' + \Phi'_{122}x_2' & \Phi'_{122}x_1' + \Phi'_{222}x_2' \end{pmatrix}\,, \tag{26}$$

and to lowest order its determinant becomes

$$\det\mathbf{J}' = \Phi'_{11}(\Phi'_{112}x_1' + \Phi'_{222}x_2')\,, \tag{27}$$

in accordance with Eq. (23). The condition $\det\mathbf{J}'(\boldsymbol{x}'^{(\mathrm{crit})}) = 0$ yields the critical curve as $\Phi'_{112}\,x_1'^{(\mathrm{crit})} + \Phi'_{222}\,x_2'^{(\mathrm{crit})} = 0$, so that with Eqs. (24) and (25), the caustic is obtained (to lowest order) as the parabola

$$y_2'^{(\mathrm{crit})} = \frac{\Phi'_{112}\Phi'_{222} - (\Phi'_{122})^2}{2(\Phi'_{11})^2\,\Phi'_{222}}\,(y_1'^{(\mathrm{crit})})^2\,. \tag{28}$$

For source positions along its symmetry axis ($y_1' = 0$), Eqs. (24) and (25) yield two images

$$\begin{aligned} x_1' &= -\frac{\Phi'_{122}}{\Phi'_{11}\Phi'_{222}}\,y_2'\,, & (29) \\ x_2' &= \pm\sqrt{\frac{2y_2'}{\Phi'_{222}}} & (30) \end{aligned}$$

for $y_2' > 0$ which degenerate into a single (critical image) for $y_2' = 0$, while there are no images for $y_2' < 0$. It follows that the normal to the caustic pointing to the inside is in the positive y_2'-direction, i.e. $\boldsymbol{n}_\mathrm{f}' = (0, 1)^\mathrm{T}$, so that in (y_1, y_2)-coordinates, $\boldsymbol{n}_\mathrm{f} = \boldsymbol{e}^{(2)}$ is the inside-pointing caustic normal at $\boldsymbol{y}_\mathrm{f}$. Neglecting y_2' against $\sqrt{y_2'}$, Eqs. (27), (29), and (30) yield the magnification due to the critical images as

$$A_\mathrm{crit}(0, y_2') = \sqrt{\frac{R_\mathrm{f}}{y_2'}}\,\Theta(y_2')\,, \tag{31}$$

where

$$R_\mathrm{f} = \frac{2}{(\Phi'_{11})^2\,|\Phi'_{222}|} > 0 \tag{32}$$

measures the strength of the strength of the fold caustic and can also be interpreted as a characteristic distance scale.

The relation given by Eq. (20) implies that derivatives of the Fermat-potential Φ with respect to x_i' and x_i are related by

$$\begin{aligned} \Phi'_{ij} &= \sum_{k,l=1}^{2} \Phi_{kl}\,\mathcal{R}_{ki}\,\mathcal{R}_{lj}\,, & (33) \\ \Phi'_{ijk} &= \sum_{l,m,n=1}^{2} \Phi_{lmn}\,\mathcal{R}_{li}\,\mathcal{R}_{mj}\,\mathcal{R}_{nk}\,, & (34) \end{aligned}$$

the first of the equations being equivalent with Eq. (21). Explicitly, the most relevant derivatives for a fold caustic read

$$\Phi'_{11} = \cos^2\theta\,\Phi_{11} + 2\,\sin\theta\,\cos\theta\,\Phi_{12} + \sin^2\theta\,\Phi_{22}\,, \tag{35}$$

$$\Phi'_{222} = \cos^3\theta\,\Phi_{111} + 3\,\sin^2\theta\,\cos\theta\,\Phi_{112} - \\ - 3\,\sin\theta\,\cos^2\theta\,\Phi_{122} + \cos^3\theta\,\Phi_{222}\,. \quad (36)$$

By inserting the explicit values for $\sin\theta$ and $\cos\theta$ given by Eq. (15), one reveals $\Phi'_{11} = \Phi_{11} + \Phi_{22}$, Eq. (22).

4 MAGNIFICATION OF SOURCE STARS

The magnification of a point source in the vicinity of a fold caustic can be decomposed into the contributions by the two critical images and the remaining images, i.e.

$$A^{\mathrm{p}}_{\mathrm{fold}}(\boldsymbol{y}) = A^{\mathrm{p}}_{\mathrm{crit}}(\boldsymbol{y}) + A^{\mathrm{p}}_{\mathrm{other}}(\boldsymbol{y})\,. \quad (37)$$

If one neglects the curvature of the caustic and any changes of the lens properties in the direction perpendicular to it, Eq. (31) together with the relation $\det\mathbf{J} = \det\mathbf{J}'$ yields the magnification for a point source at $\boldsymbol{y}$ due to the critical images as

$$A^{\mathrm{p}}_{\mathrm{crit}}(y_\perp; R_{\mathrm{f}}) = \left(\frac{y_\perp}{R_{\mathrm{f}}}\right)^{-1/2} \Theta(y_\perp)\,, \quad (38)$$

where $y_\perp = (\boldsymbol{y} - \boldsymbol{y}_{\mathrm{f}})\cdot\boldsymbol{n}_{\mathrm{f}}$ is the distance perpendicular to the caustic (c.f. Schneider & Weiß 1986; Schneider et al. 1992, p.186f.; Albrow et al. 1999b). For the validity and limits of this approximation, the reader is referred to Gaudi & Petters (2002).

Let us consider a circular source star with radius $\rho_\star$ and surface brightness $I^{(s)}(\rho) = \overline{I}^{(s)}\,\xi^{(s)}(\rho)$ for a filter s as function of the fractional radius $0 \leqslant \rho \leqslant 1$, where $\overline{I}^{(s)}$ denotes the average value, and $\xi^{(s)}(\rho)$ is a dimensionless function describing the radial stellar brightness profile, which is normalized to yield unity if integrated over the source, i.e.

$$\int_0^1 \xi^{(s)}(\rho)\,\rho\,\mathrm{d}\rho = \frac{1}{2}\,. \quad (39)$$

With $I^{(s)}(\rho)$ being composed of the specific intensities $I^\lambda(\rho)$ for the wavelength λ by means of the transmission function $B^{(s)}(\lambda)$ as

$$I^{(s)}(\rho) = \int_0^\infty I^\lambda(\rho)\,B^{(s)}(\lambda)\,d\lambda\,, \quad (40)$$

and $I^\lambda(\rho) = \overline{I}^\lambda\,\xi^\lambda(\rho)$, where $\overline{I}^\lambda$ denotes the average intensity and $\xi^\lambda(\rho)$ a dimensionless normalized profile function for the specific wavelength, one obtains

$$\xi^{(s)}(\rho) = \frac{\int_0^\infty \overline{I}^\lambda B^{(s)}(\lambda)\,\xi^\lambda(\rho)\,\mathrm{d}\lambda}{\int_0^\infty \overline{I}^\lambda B^{(s)}(\lambda)\,\mathrm{d}\lambda}\,. \quad (41)$$

For the source being centered at $\boldsymbol{y}$, one obtains the magnification by convolving Eq. (38) with the brightness profile $\xi^{(s)}(\rho)$, yielding

$$A_{\mathrm{crit}}(y_\perp, \rho_\star; R_{\mathrm{f}}; \xi^{(s)}) = A^0_{\mathrm{crit}}(y_\perp/\rho_\star, \rho_\star/R_{\mathrm{f}}; \xi^{(s)}) \\ = \left(\frac{R_{\mathrm{f}}}{\rho_\star}\right)^{1/2} G^\star_{\mathrm{f}}\left(1 + \frac{y_\perp}{\rho_\star}; \xi^{(s)}\right), \quad (42)$$

where $G^\star_{\mathrm{f}}$ is a universal fold-caustic profile function depending on the brightness profile $\xi^{(s)}$ of the source given by (Schneider & Weiß 1987)

$$G^\star_{\mathrm{f}}(\eta; \xi^{(s)}) = \frac{2}{\pi} \int_{\max(1-\eta,-1)}^{\max(1-\eta,1)} \frac{1}{\sqrt{\rho_\perp + \eta - 1}} \times \\ \times \int_0^{\sqrt{1-\rho_\perp^2}} \xi^{(s)}\left(\sqrt{\rho_\perp^2 + \rho_\parallel^2}\right) \mathrm{d}\rho_\parallel\,\mathrm{d}\rho_\perp\,. \quad (43)$$

In contrast to several previous papers, η is defined so that the source is completely outside the caustic for $\eta < 0$, where $G^\star_{\mathrm{f}}(\eta; \xi^{(s)}) = 0$, completely inside the caustic for $\eta > 2$, and its center crosses the caustic for $\eta = 1$. As can be seen directly from Eq. (42), $A_{\mathrm{crit}}(y_\perp, \rho_\star; R_{\mathrm{f}}; \xi^{(s)})$ depends only on the two ratios $y_\perp/\rho_\star$ and $\rho_\star/R_{\mathrm{f}}$. Explicit forms of $G^\star_{\mathrm{f}}$ for selected brightness profiles $\xi^{(s)}$ will be discussed in Sect. 5.

Compared to $A^{\mathrm{p}}_{\mathrm{crit}}$, the magnification due to the remaining, non-critical images is varying slowly in the vicinity of a caustic, so that it can be expanded as

$$A^{\mathrm{p}}_{\mathrm{other}}(\boldsymbol{y}) = A_{\mathrm{f}} + (\boldsymbol{y} - \boldsymbol{y}_{\mathrm{f}})\cdot(\boldsymbol{\nabla}A)_{\mathrm{f}}\,, \quad (44)$$

where $A_{\mathrm{f}} = A^{\mathrm{p}}_{\mathrm{other}}(\boldsymbol{y}_{\mathrm{f}})$ and $(\boldsymbol{\nabla}A)_{\mathrm{f}} = \boldsymbol{\nabla}A^{\mathrm{p}}_{\mathrm{other}}(\boldsymbol{y}_{\mathrm{f}})$. It is assumed that $(\boldsymbol{\nabla}A)_{\mathrm{f}} \neq 0$, while otherwise the use of higher-order terms in the expansion would be indicated.[10] Both A_{f} and $(\boldsymbol{\nabla}A)_{\mathrm{f}}$ can be expressed by means of derivatives of the Fermat potential Φ evaluated at the $\tilde{N}$ non-critical images $\boldsymbol{x}^{(i)}$ of the source at $\boldsymbol{y}_{\mathrm{f}}$. As outlined in detail by Witt & Mao (1995), the lens equation for a binary lens can be written as 5th-order complex polynomial in $z = x_1 + \mathrm{i}\,x_2$ which can be solved numerically for the the images $z^{(i)} = x_1^{(i)} + \mathrm{i}\,x_2^{(i)}$ by standard root-finding routines. While A_{f} is simply given by

$$A_{\mathrm{f}} = \sum_{i=1}^{\tilde{N}} \frac{1}{|\Phi_{11}\Phi_{22} - (\Phi_{12})^2|}\,, \quad (45)$$

the gradient $(\boldsymbol{\nabla}A)_{\mathrm{f}}$ can be determined as follows.

For an image at $\boldsymbol{x}_0$ and the corresponding source at $\boldsymbol{y}_0$, derivatives with respect to the components of $\boldsymbol{x}$ and $\boldsymbol{y}$ are related by

$$\boldsymbol{\nabla}_{\boldsymbol{y}} = \mathbf{J}^{-1}(\boldsymbol{x}_0)\,\boldsymbol{\nabla}_{\boldsymbol{x}}\,, \quad (46)$$

so that $(\boldsymbol{\nabla}A)_{\mathrm{f}}$ reads

$$(\boldsymbol{\nabla}A)_{\mathrm{f}} = \sum_{i=1}^{\tilde{N}} \mathbf{J}^{-1}(\boldsymbol{x}^{(i)})\,\boldsymbol{\nabla}_{\boldsymbol{x}}|\mu(\boldsymbol{x}^{(i)})| \\ = -\sum_{i=1}^{\tilde{N}} \frac{\mathrm{sign}(\det\mathbf{J}(\boldsymbol{x}^{(i)}))}{|\det\mathbf{J}(\boldsymbol{x}^{(i)})|^2}\,\mathbf{J}^{-1}(\boldsymbol{x}^{(i)})\,\boldsymbol{\nabla}_{\boldsymbol{x}}\det\mathbf{J}(\boldsymbol{x}^{(i)})\,. \quad (47)$$

With

$$\mathbf{J}^{-1} = \frac{1}{\det\mathbf{J}}\begin{pmatrix} \Phi_{22} & -\Phi_{12} \\ -\Phi_{12} & \Phi_{11} \end{pmatrix} \quad (48)$$

and

[10] The condition $(\boldsymbol{\nabla}A)_{\mathrm{f}} \neq 0$ is thought to hold for all fold singularities of binary lenses, since $(\boldsymbol{\nabla}A)_{\mathrm{f}} = 0$ would require a symmetry of A_{f} to spatial variations in directions both parallel and perpendicular to the line connecting the two lens objects, which should only be achievable for source positions in between the lens objects, where however a saddlepoint rather than a maximum or minimum is expected.

$$\boldsymbol{\nabla}_{\boldsymbol{x}} \det \mathbf{J} = \begin{pmatrix} \Phi_{11}\Phi_{122} - 2\,\Phi_{12}\Phi_{112} + \Phi_{22}\Phi_{111} \\ \Phi_{11}\Phi_{222} - 2\,\Phi_{12}\Phi_{122} + \Phi_{22}\Phi_{112} \end{pmatrix}, \qquad (49)$$

$(\boldsymbol{\nabla} A)_{\rm f}$ expressed by means of the derivatives of the Fermat potential Φ becomes

$$(\boldsymbol{\nabla} A)_{\rm f} = -\sum_{i=1}^{\tilde{N}} \frac{1}{|\Phi_{11}\Phi_{22} - (\Phi_{12})^2|^3} \times \times \begin{pmatrix} -\Phi_{11}\Phi_{22}\Phi_{222} + \\ \quad + [\Phi_{11}\Phi_{22} + 2\,(\Phi_{12})^2]\,\Phi_{122} - \\ \quad - 3\,\Phi_{12}\Phi_{22}\Phi_{112} + \Phi_{22}^2\Phi_{111} \\ \Phi_{11}^2\Phi_{222} - 3\,\Phi_{11}\,\Phi_{12}\,\Phi_{122} + \\ \quad + [\Phi_{11}\Phi_{22} + 2\,(\Phi_{12})^2]\,\Phi_{112} - \\ \quad - \Phi_{12}\Phi_{22}\Phi_{111} \end{pmatrix}. \qquad (50)$$

Due to symmetry, the magnification of an extended circular source $A_{\rm other}(\boldsymbol{y}, \rho_\star; \xi^{(s)})$, obtained by integration of the convolution of the magnification $A^{\rm P}_{\rm other}$ as given by Eq. (44) with the radial source brightness profile, turns out to be equal to that of a point source at its center, i.e. $A_{\rm other}(\boldsymbol{y}, \rho_\star; \xi^{(s)}) = A^{\rm P}_{\rm other}(\boldsymbol{y})$ unless the source size exceeds the range for which the expansion is a fair approximation, so that the total magnification of an extended circular source reads $A_{\rm fold}(\boldsymbol{y}, \rho_\star; \xi^{(s)}) = A_{\rm crit}(\boldsymbol{y}, \rho_\star; \xi^{(s)}) + A^{\rm P}_{\rm other}(\boldsymbol{y})$.

5 LIMB DARKENING

With ϑ denoting the angle between the normal to the stellar surface and the direction to the observer, so that $\cos\vartheta = \sqrt{1-\rho^2}$, normalized brightness profile functions

$$\xi^{(s)}_{\{p\}}(\rho) = (1 + p/2)\,(1-\rho^2)^{p/2} \qquad (51)$$

are proportional to $\cos^p\vartheta$, and their linear superposition

$$\xi^{(s)}(\rho; \Gamma^{(s)}_{\{p_1\}} \ldots \Gamma^{(s)}_{\{p_{k_{\rm I}}\}}) = 1 + \sum_{i=1}^{k_{\rm I}} \Gamma^{(s)}_{\{p_i\}} \left[\xi^{(s)}_{\{p_i\}}(\rho) - 1\right], \qquad (52)$$

where $p_i > 0$, provides a popular class of models for limb darkening. The contribution of individual base profiles $\xi^{(s)}_{\{p_i\}}(\rho)$ to the full brightness profile function $\xi^{(s)}(\rho)$ is measured by the $k_{\rm I}$ limb-darkening coefficients $0 \leqslant \Gamma^{(s)}_{\{p_i\}} \leqslant 1$, which moreover have to fulfill the condition

$$\sum_{i=1}^{k_{\rm I}} \Gamma^{(s)}_{\{p_i\}} \leqslant 1\,. \qquad (53)$$

The stellar brightness profiles $\xi^{(s)}_{\{p\}}$ for uniform brightness ($p = 0$), square-root ($p = 1/2$), linear ($p = 1$) and quadratic limb darkening ($p = 2$) as a function of the fractional radius ρ are shown in Fig. 1. In general, larger powers of p provide stronger limb darkening.

By inserting the brightness profile $\xi^{(s)}_{\{p\}}(\rho)$ into Eq. (43), one obtains its fold-caustic magnification function $G^\star_{{\rm f},\{p\}}(\eta) \equiv G^\star_{\rm f}(\eta; \xi^{(s)}_{\{p\}})$ as (Schneider & Weiß 1987)

$$G^\star_{{\rm f},\{p\}}(\eta) = \frac{1}{\sqrt{\pi}}\,\frac{(1+\frac{p}{2})!}{(\frac{1+p}{2})!} \int\limits_{\max(1-\eta,-1)}^{\max(1-\eta,1)} \frac{(1-x^2)^{\frac{1+p}{2}}}{\sqrt{x+\eta-1}}\,{\rm d}x\,. \qquad (54)$$

For even p (including $p = 0$), the fold-caustic magnification function $G^\star_{{\rm f},\{p\}}$ can be expressed by means of the complete elliptical integrals of the first and second kind, $K(x)$ and $E(x)$, respectively (e.g. Gradshteyn & Ryzhik 1994), while $G^\star_{{\rm f},\{p\}}$ becomes an analytical function for odd p. For uniformly bright sources ($p = 0$), one obtains (Schneider & Weiß 1987)

$$G^\star_{{\rm f},\{0\}}(\eta) = \begin{cases} 0 & \text{for} \quad \eta \leqslant 0 \\ \frac{4\sqrt{2}}{3\pi}\left[(2-\eta)\,K\left(\sqrt{\frac{\eta}{2}}\right) - \right. & \\ \quad \left. -2\,(1-\eta)\,E\left(\sqrt{\frac{\eta}{2}}\right)\right] & \text{for} \quad 0 < \eta < 2 \\ \frac{8}{3\pi}\sqrt{\eta}\left[(2-\eta)\,K\left(\sqrt{\frac{2}{\eta}}\right) - \right. & \\ \quad \left. -(1-\eta)\,E\left(\sqrt{\frac{2}{\eta}}\right)\right] & \text{for} \quad \eta \geqslant 2 \end{cases}, \qquad (55)$$

while for linear limb darkening ($p = 1$) the evaluation of Eq. (54) yields (Schneider & Wagoner 1987)

$$G^\star_{{\rm f},\{1\}}(\eta) = \begin{cases} 0 & \text{for} \quad \eta \leqslant 0 \\ \frac{2}{5}\,(5-2\eta)\,\eta^{3/2} & \text{for} \quad 0 < \eta \leqslant 2 \\ \frac{2}{5}\left[(5-2\eta)\,\eta^{3/2} + \right. & \\ \quad \left. +\ (1+2\eta)\,(\eta-2)^{3/2}\right] & \text{for} \quad \eta > 2 \end{cases}. \qquad (56)$$

The fold-caustic magnification functions $G^\star_{{\rm f},\{p\}}$ for uniformly bright sources ($p = 0$), square-root ($p = 1/2$), linear ($p = 1$) and quadratic limb darkening ($p = 2$) are shown in Fig. 2. With the stellar surface brightness vanishing at the limb for all power-law profiles with $p > 0$, the slope of $G^\star_{{\rm f},\{p\}}$ becomes zero when the stellar limb touches the caustic from the outside ($\eta = 0$), In contrast, there is a slope discontinuity at this phase for $p = 0$ and therefore for all brightness profiles that involve a non-zero constant brightness term. As the source enters the caustic, the magnification rises to a peak and thereafter falls asymptotically with the inverse square root of its perpendicular distance to the caustic. The position of the peak depends on the brightness profile and occurs for the source center being inside the caustic. With more light being concentrated near the source center, stronger limb darkening can account for fold-caustic peak magnifications similar to that for less limb-darkened but smaller sources. On entering the caustic, stronger limb darkening produces less steep initial rises of the magnification, while

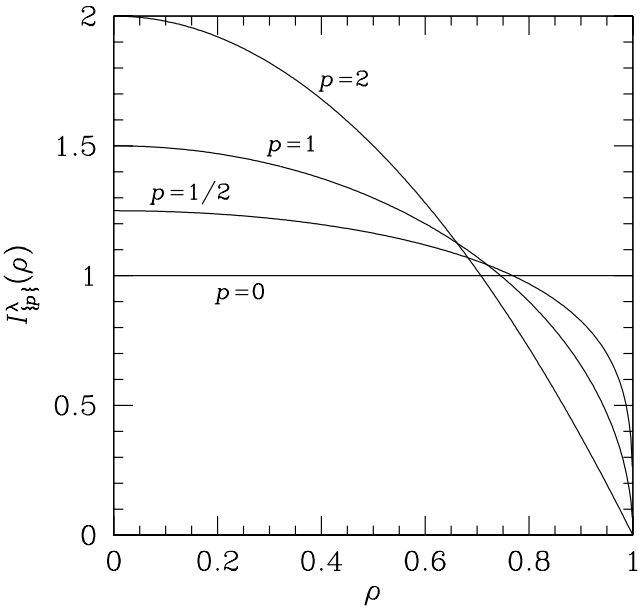

Figure 1. Stellar brightness profiles $\xi^{(s)}_{\{p\}}(\rho) = (1+p/2)\,(1-\rho^2)^{p/2}$ as a function of the fractional radius ρ for source stars with uniform brightness ($p = 0$), square-root ($p = 1/2$), linear ($p = 1$), and quadratic ($p = 2$) limb darkening.

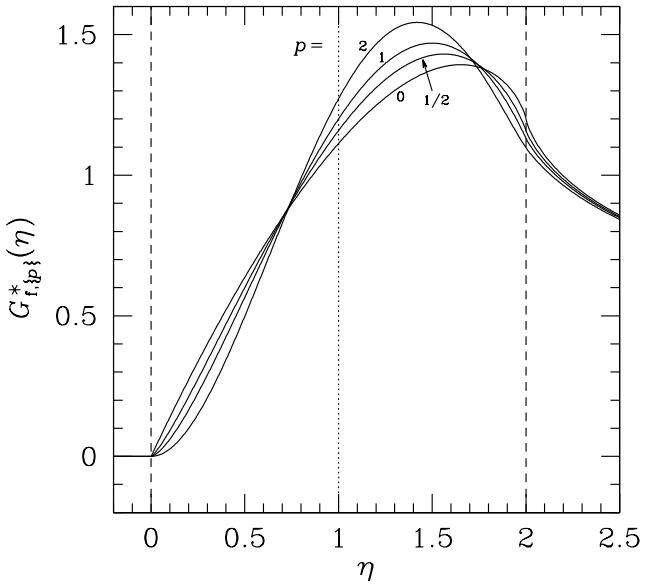

Figure 2. Universal fold-caustic magnification function $G^\star_{\mathrm{f},\{p\}}(\eta)$ for selected source brightness profiles following power-laws in $\cos\vartheta = \sqrt{1-\rho^2}$ of the form $\xi^{(s)}_{\{\mathrm{p}\}}(\rho) = (1+p/2)\,(1-\rho^2)^{p/2}$: Uniform brightness ($p=0$), square-root ($p=1/2$), linear ($p=1$), and quadratic ($p=2$) limb darkening.

steeper rises occur before a narrower peak at higher magnification is reached for a smaller distance of the source center from the caustic. After the peak, the magnification for extended sources exceeds that of a point source, where the difference increases for weaker limb darkening.

For more details about the fold-caustic magnification function $G^\star_{\mathrm{f},\{p\}}$, the reader is referred to Rhie & Bennett (1999), while more about the extraction of limb-darkening parameters from the observed data during a fold-caustic passage event can be found in two recent papers by Dominik (2004a,b).

6 LIGHTCURVES NEAR FOLDS

Let the center of the source cross the caustic at time t_f and let $t^\star_\mathrm{f}$ denote the point of time when the source begins to enter or finishes to exit the caustic. If the source brightness does not vanish at the stellar limb, $G^\star_\mathrm{f}(\eta;\xi^{(s)})$ involves a slope discontinuity at $\eta=0$, producing a characteristic feature in the lightcurve at time $t^\star_\mathrm{f}$, whereas t_f is much less easily recognizable from the lightcurve. The choice of $t^\star_\mathrm{f}$ as reference point rather than t_f constitutes an importance difference to the discussion presented by Albrow et al. (1999b) and is the key point for avoiding strong correlations between model parameters. With $t^\perp_\star = \pm\,(t_\mathrm{f}-t^\star_\mathrm{f}) \geqslant 0$ (throughout the paper, the upper sign will refer to a caustic entry, while the lower sign will refer to a caustic exit), the source crosses the caustic during the timespan $2\,t^\perp_\star$. Let $0<\phi<\pi$ denote the angle from the caustic tangent to the source trajectory, and $t_\mathrm{E}>0$ denote the timespan in which the source moves by a unit distance. During the time $t^\perp_\mathrm{E} = t_\mathrm{E}/(\sin\phi)$, the source therefore moves by a unit distance perpendicular to the caustic, and $t^\perp_\star = \rho_\star\, t^\perp_\mathrm{E}$, so that

$$y_\perp = \pm\,\frac{t-t_\mathrm{f}}{t^\perp_\mathrm{E}} = \pm\,\rho_\star\,\frac{t-t_\mathrm{f}}{t^\perp_\star} = \rho_\star\,\left(\pm\,\frac{t-t^\star_\mathrm{f}}{t^\perp_\star} - 1\right)\,. \qquad (57)$$

With $\hat{t}$ denoting an arbitrarily chosen unit time, and

$$t_\mathrm{r} \equiv R_\mathrm{f}\,t^\perp_\mathrm{E} > 0 \qquad (58)$$

a characteristic caustic rise time, one can define a caustic rise parameter

$$\zeta_\mathrm{f} \equiv \sqrt{\frac{t_\mathrm{r}}{\hat{t}}} > 0\,. \qquad (59)$$

With these definitions, Eq. (42) yields the magnification due to the critical images as

$$\begin{aligned} A_\mathrm{crit}(t) &\equiv A^0_\mathrm{crit}\left(\pm\,\frac{t-t^\star_\mathrm{f}}{t^\perp_\star} - 1, \frac{t^\perp_\star}{\zeta_\mathrm{f}^2\,\hat{t}};\xi^{(s)}\right) \\ &= \zeta_\mathrm{f}\,\left(\frac{\hat{t}}{t^\perp_\star}\right)^{1/2} G^\star_\mathrm{f}\left(\pm\,\frac{t-t^\star_\mathrm{f}}{t^\perp_\star};\xi^{(s)}\right)\,. \end{aligned} \qquad (60)$$

The singularity in this expression for $t^\perp_\star = 0$ (point source) can be avoided by defining a function

$$\hat{G}^\star_\mathrm{f}\left(\hat{y}^\star_\perp,\hat{\rho}^\perp_\star;\xi^{(s)}\right) = \begin{cases} \left(\hat{\rho}^\perp_\star\right)^{-1/2} \times \\ \quad \times\, G^\star_\mathrm{f}\left(\hat{y}^\star_\perp/\hat{\rho}^\perp_\star;\xi^{(s)}\right) \\ \qquad \text{for} \quad \hat{\rho}^\perp_\star \neq 0 \\ \left(\hat{y}^\star_\perp\right)^{-1/2}\,\Theta\left(\hat{y}^\star_\perp\right) \\ \qquad \text{for} \quad \hat{\rho}^\perp_\star = 0 \end{cases}\,, \qquad (61)$$

which is continuous in $t^\perp_\star = 0$, i.e.

$$\begin{aligned} &\lim_{t^\perp_\star\to 0} \hat{G}^\star_\mathrm{f}\left(\pm\,\frac{t-t^\star_\mathrm{f}}{\hat{t}},\frac{t^\perp_\star}{\hat{t}};\xi^{s)}\right) = \\ &\quad = \hat{G}^\star_\mathrm{f}\left(\pm\,\frac{t-t^\star_\mathrm{f}}{\hat{t}},0;\xi^{(s)}\right)\,, \end{aligned} \qquad (62)$$

and allows the magnification due to the critical images to be expressed as

$$A_\mathrm{crit}(t) = \zeta_\mathrm{f}\,\hat{G}^\star_\mathrm{f}\left(\pm\,\frac{t-t^\star_\mathrm{f}}{\hat{t}},\frac{t^\perp_\star}{\hat{t}};\xi^{(s)}\right)\,. \qquad (63)$$

Consider n lightcurves being observed and let $F^{(s)}_\mathrm{S} > 0$ and $F^{(s)}_\mathrm{B}$ denote the fluxes of the source and the background, respectively, for the s-th lightcurve, so that the blend ratio is given by $g^{(s)} = F^{(s)}_\mathrm{B}/F^{(s)}_\mathrm{S}$ and the baseline flux is $F^{(s)}_\mathrm{base} = F^{(s)}_\mathrm{S} + F^{(s)}_\mathrm{B}$. In analogy to the spatial expansion of the magnification $A^\mathrm{p}_\mathrm{other}$ due to the non-critical images as given by Eq. (44), its temporal expansion around $t^\star_\mathrm{f}$ reads

$$A^\mathrm{p}_\mathrm{other}(t) \simeq A^\star_\mathrm{f} + (t-t^\star_\mathrm{f})\dot{A}^\star_\mathrm{f}\,, \qquad (64)$$

where $A^\star_\mathrm{f} = A^\mathrm{p}_\mathrm{other}(t^\star_\mathrm{f})$ and $\dot{A}^\star_\mathrm{f} = \dot{A}^\mathrm{p}_\mathrm{other}(t^\star_\mathrm{f})$. The relations between the coefficients $A^\star_\mathrm{f}$, $\dot{A}^\star_\mathrm{f}$, A_f, and $(\boldsymbol{\nabla}A)_\mathrm{f}$ will be discussed In Section 7.

Let us define

$$F^{(s)}_\mathrm{r} \equiv \zeta_\mathrm{f}\,F^{(s)}_\mathrm{S} > 0\,, \qquad (65)$$

$$\hat{\omega}^\star_\mathrm{f} \equiv \pm\,\frac{\dot{A}^\star_\mathrm{f}}{\zeta_\mathrm{f}}\,, \qquad (66)$$

and the flux at time $t^\star_\mathrm{f}$ as

$$F^{\star(s)}_\mathrm{f} \equiv F^{(s)}_\mathrm{S}\,A^\star_\mathrm{f} + F^{(s)}_\mathrm{B} = F^{(s)}_\mathrm{S}\,(A^\star_\mathrm{f} + g^{(s)})\,. \qquad (67)$$

Using the above definitions, the total flux $F^{(s)}_\mathrm{fold}(t) = F^{(s)}_\mathrm{S}\,[A_\mathrm{crit}(t) + A^\mathrm{p}_\mathrm{other}(t)] + F^{(s)}_\mathrm{B}$ for the s-th lightcurve takes the form

$$F^{(s)}_\mathrm{fold}(t) = F^{(s)}_\mathrm{r}\,\left[\hat{G}^\star_\mathrm{f}\left(\pm\,\frac{t-t^\star_\mathrm{f}}{\hat{t}},\frac{t^\perp_\star}{\hat{t}};\xi^{(s)}\right)\,\pm\right.$$

$$\pm\,\hat{\omega}_{\rm f}^{\star}\,(t-t_{\rm f}^{\star})\Big]+F_{\rm f}^{\star\,(s)}\,. \qquad (68)$$

A fit to the n observed lightcurves therefore involves the $3+2n$ parameters $t_{\rm f}^{\star}$, $t_{\star}^{\perp}>0$, $F_{\rm r}^{(s)}>0$, $F_{\rm f}^{\star\,(s)}$, and $\hat{\omega}_{\rm f}^{\star}$. The fluxes $F_{\rm r}^{(s)}$ measure the asymptotic behaviour of the lightcurve for source positions towards the inside of the caustic (i.e. for $t\to\pm\infty$) and can be interpreted as the flux of the two critical images that are produced at the time $t=t_{\rm f}\pm\hat{t}=t_{\rm f}^{\star}\pm(t_{\star}^{\perp}+\hat{t}\,)$ if the extended source is replaced by a point source at its center, where the chosen point of time corresponds to a unit time after the source center enters or before it exits the caustic which itself takes place at $t=t_{\rm f}\pm t_{\star}^{\perp}$. The parameter $\hat{\omega}_{\rm f}^{\star}$ describes the temporal variation of $A_{\rm other}^{\rm P}$, where $\pm\,\hat{\omega}_{\rm f}^{\star}$ measures the rate of the corresponding change of flux in units of $F_{\rm r}^{(s)}$ with positive time. Since the change of caustic properties in the direction parallel to it has been neglected, the lightcurve is affected by the transverse motion only. The observable width of the caustic passage given by $t_{\star}^{\perp}$ is the product of the source size parameter $\rho_{\star}$ and the time-scale of transverse motion $t_{\rm E}^{\perp}$, whereas neither of the two latter quantities are observables themselves.

The meaning of the model parameters $t_{\rm f}^{\star}$, $t_{\star}^{\perp}$, $F_{\rm r}^{(s)}$, $F_{\rm f}^{\star\,(s)}$, and $\hat{\omega}_{\rm f}^{\star}$ is illustrated in Fig. 3. For observed lightcurves, initial guesses for these parameters can easily be obtained from recognizable features. The point of time $t_{\rm f}^{\star}$ is indicated by the arising slope discontinuity, and $F_{\rm f}^{\star(s)}$ is obtained as the flux at $t_{\rm f}^{\star}$. The duration of the caustic passage $2\,t_{\star}^{\perp}$ extends approximately between the slope discontinuity at $t_{\rm f}^{\star}$ and the change of sign of the curvature on the other side of the caustic peak. With two fluxes $F_1^{(s)}=F_{\rm fold}^{(s)}(t_1)$ and $F_2^{(s)}=F_{\rm fold}^{(s)}(t_2)$ taken at two points of time t_1 and t_2 in the region where the source is located inside the caustic and can be fairly approximated by a point source and the rate of change of flux $\dot{F}_{\rm f}^{\star\,(s)}$ of the non-critical images at $t_{\rm f}^{\star}$ (obtained as the limit of the tangent for $t\to t_{\rm f}^{\star}$ from the outside), one obtains

$$\begin{aligned} F_{\rm r}^{(s)} \;=\; & \left[(t_1-t_{\rm f}^{\star})\sqrt{\frac{\hat{t}}{\pm(t_2-t_{\rm f}^{\star})-t_{\star}^{\perp}}}\;-\right. \\ & \left.-\;(t_2-t_{\rm f}^{\star})\sqrt{\frac{\hat{t}}{\pm(t_1-t_{\rm f}^{\star})-t_{\star}^{\perp}}}\right]\Bigg/ \\ & \Bigg/\left[(F_2^{(s)}-F_{\rm f}^{\star\,(s)})\,(t_1-t_{\rm f}^{\star})\;-\right. \\ & \left.-\;(F_1^{(s)}-F_{\rm f}^{\star\,(s)})\,(t_2-t_{\rm f}^{\star})\right]. \end{aligned} \qquad (69)$$

Finally, the slope of any chosen lightcurve k for the source just outside the caustic denoted by $\dot{F}_{\rm f}^{\star\,(k)}$ yields $\hat{\omega}_{\rm f}^{\star}=\pm\dot{F}_{\rm f}^{\star\,(k)}/F_{\rm r}^{(k)}$.

In the absence of blending, $F_{\rm B}^{(s)}=0$ for all s, so that Eqs. (65) and (67) yield a constant ratio between $F_{\rm f}^{\star(s)}$ and $F_{\rm r}^{(s)}$, namely

$$g_{\rm f}^{\star}\equiv\frac{F_{\rm f}^{\star(s)}}{F_{\rm r}^{(s)}}=\frac{A_{\rm f}^{\star}}{\zeta_{\rm f}}>0\,. \qquad (70)$$

In this case, modelling the lightcurve to the observed data involves $4+n$ independent parameters, which can be chosen as $t_{\rm f}^{\star}$, $t_{\star}^{\perp}>0$, $g_{\rm f}^{\star}>0$, $F_{\rm f}^{\star\,(s)}>0$, and $\hat{\omega}_{\rm f}^{\star}$.

While in the case of difference-imaging, the flux $F_{\rm B}^{(s)}$ represents the total background and can have either sign, it is restricted to $F_{\rm B}^{(s)}\geqslant 0$ for standard photometry. The conditions $F_{\rm S}^{(s)}>0$ and $A_{\rm f}^{\star}>1$ imply $F_{\rm fold}^{(s)}(t)>0$ for all t in this case, so that Eq. (67) requires $F_{\rm f}^{\star(s)}>0$. Therefore, a model parameter $F_{\rm f}^{\star(k)}\leqslant 0$ for the k-th lightcurve implies a negative background flux $F_{\rm B}^{(k)}$.

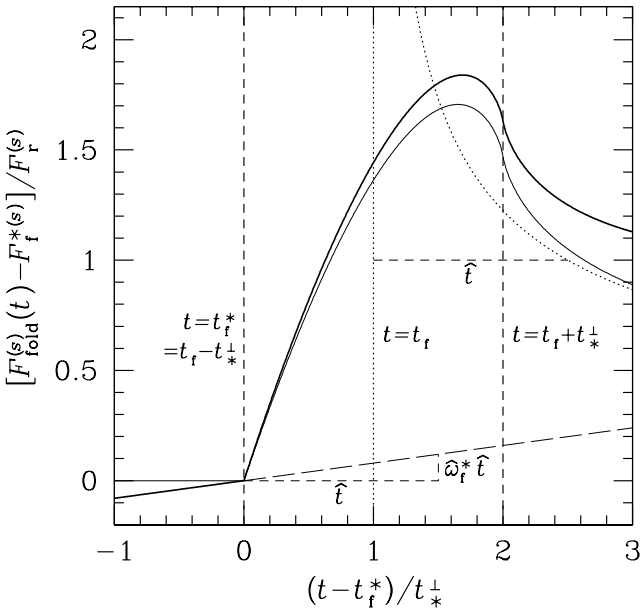

Figure 3. Typical lightcurve for a uniformly bright source entering a fold caustic (bold solid line) which illustrates the physical meaning of the model parameters $t_{\rm f}^{\star}$, $t_{\star}^{\perp}>0$, $F_{\rm r}^{(s)}>0$, $F_{\rm f}^{\star(s)}$, and $\hat{\omega}_{\rm f}^{\star}$. For this example, $t_{\star}^{\perp}=2/3\,\hat{t}$ and $\hat{\omega}_{\rm f}^{\star}=0.08$ have been chosen. Also shown are lightcurves with $\hat{\omega}_{\rm f}^{\star}=0$ for the uniformly bright extended source (light solid line) and the corresponding point source (dotted line). The long-dashed line shows the contribution by the variation of $A_{\rm other}^{\rm P}(t)$.

For sufficiently small $\pm\,\hat{\omega}_{\rm f}^{\star}\,(t-t_{\rm f}^{\star})$, $F_{\rm fold}^{(s)}$ as given by Eq. (68) violates the condition $F_{\rm fold}^{(s)}(t)>0$. Although the approximation of $A_{\rm other}(t)$ by its expansion around $t=t_{\rm f}^{\star}$ only holds for $|t-t_{\rm f}^{\star}|\ll\left|A_{\rm f}^{\star}/\dot{A}_{\rm f}^{\star}\right|$, evaluations outside this region may be attempted during a parameter search. Negative fluxes prohibit the calculation of a corresponding magnitude which can however be avoided by using a modified expansion of $A_{\rm other}^{\rm P}$ involving an exponential function rather than a linear function, which is a purely technical modification and has negligible effect on the lightcurve in the vicinity of the caustic passage. Let us therefore expand $A_{\rm other}^{\rm P}$ as

$$A_{\rm other}^{\rm P}(t)\simeq A_{\rm f}^{\star}+\alpha_{\rm f}\left(\exp\left\{\frac{\dot{A}_{\rm f}^{\star}\,(t-t_{\rm f}^{\star})}{\alpha_{\rm f}}\right\}-1\right), \qquad (71)$$

where $\alpha_{\rm f}>0$, so that the local properties $A_{\rm other}^{\rm P}(t_{\rm f}^{\star})=A_{\rm f}^{\star}$ and $\dot{A}_{\rm other}^{\rm P}(t_{\rm f}^{\star})=\dot{A}_{\rm f}^{\star}$ are fulfilled.

In analogy to Eq. (70), one can define

$$g_{\rm f}^{\star\,(s)}\equiv\frac{F_{\rm f}^{\star(s)}}{F_{\rm r}^{(s)}}=\frac{A_{\rm f}^{\star}+g^{(s)}}{\zeta_{\rm f}}>0 \qquad (72)$$

and

$$g_{\rm f,min}^{\star}\equiv\min_{1\leqslant s\leqslant n}\left\{g_{\rm f}^{\star\,(s)}\right\}>0\,, \qquad (73)$$

which corresponds to the lightcurve involving the smallest blend ratio.

With $\alpha_{\rm f}=\zeta_{\rm f}\,g_{\rm f,min}^{\star}$ and $\hat{\omega}_{\rm f}^{\star}$ as defined by Eq. (66), the total flux for the s-th lightcurve reads

$$\tilde{F}_{\rm fold}^{(s)}(t)=F_{\rm r}^{(s)}\,\left[\hat{G}_{\rm f}^{\star}\left(\pm\,\frac{t-t_{\rm f}^{\star}}{\hat{t}},\frac{t_{\star}^{\perp}}{\hat{t}};\xi^{(s)}\right)\;+\right.$$

$$+\ g^{\star}_{\mathrm{f,min}}\ \left(\exp\left\{\pm\,\frac{\hat{\omega}^{\star}_{\mathrm{f}}\,(t-t^{\star}_{\mathrm{f}})}{g^{\star}_{\mathrm{f,min}}}\right\}-1\right)\Bigg]+F^{\star\,(s)}_{\mathrm{f}}\,. \quad (74)$$

With the corresponding magnitude being defined as

$$m^{(s)}_{\mathrm{fold}}(t)=m^{\star\,(s)}_{\mathrm{f}}-2.5\,\lg\frac{\tilde{F}^{(s)}_{\mathrm{fold}}(t)}{F^{\star\,(s)}_{\mathrm{f}}}\,, \quad (75)$$

where, in analogy to $F^{\star\,(s)}_{\mathrm{f}}$, $m^{\star\,(s)}_{\mathrm{f}}$ denotes the magnitude at time $t^{\star}_{\mathrm{f}}$, the magnitude near a fold-caustic passage takes the form

$$\begin{aligned} m^{(s)}_{\mathrm{fold}}(t) &= m^{\star\,(s)}_{\mathrm{f}}\ - \\ &-2.5\,\lg\left\{1+\frac{1}{g^{\star\,(s)}_{\mathrm{f}}}\,\left[\hat{G}^{\star}_{\mathrm{f}}\left(\pm\,\frac{t-t^{\star}_{\mathrm{f}}}{\hat{t}},\,\frac{t^{\perp}_{\star}}{\hat{t}};\xi^{(s)}\right)\ +\right.\right. \\ &\left.\left.+\ g^{\star}_{\mathrm{f,min}}\ \left(\exp\left\{\pm\,\frac{\hat{\omega}^{\star}_{\mathrm{f}}\,(t-t^{\star}_{\mathrm{f}})}{g^{\star}_{\mathrm{f,min}}}\right\}-1\right)\right]\right\}\,, \end{aligned} \quad (76)$$

and lightcurve models involve the $3+2n$ parameters $t^{\star}_{\mathrm{f}}$, $t^{\perp}_{\star}>0$, $g^{\star\,(s)}_{\mathrm{f}}>0$, $m^{\star\,(s)}_{\mathrm{f}}$ and $\hat{\omega}^{\star}_{\mathrm{f}}$ which reduce to the $4+n$ parameters $t^{\star}_{\mathrm{f}}$, $t^{\perp}_{\star}>0$, $g^{\star}_{\mathrm{f}}>0$, $m^{\star\,(s)}_{\mathrm{f}}$ and $\hat{\omega}^{\star}_{\mathrm{f}}$ in the absence of blending.

7 FULL LIGHTCURVE AND BINARY LENS MODEL

7.1 Constraining the parameter space

For a galactic microlensing event involving an extended source at distance D_{S} and a binary lens with total mass M at distance D_{L}, let us choose the angular Einstein radius θ_{E}, defined by Eq. (1), as the unitlength of our coordinates (x_1,x_2) and (y_1,y_2). Usually, the resulting lightcurve is characterized by the $7+2n$ model parameters (d, q, u_0, α, t_0, t_{E}, $\rho_{\star}$, $F^{(s)}_{\mathrm{S}}$, $F^{(s)}_{\mathrm{B}}$) being described in the following. The binary lens itself is characterized by the angular separation of its components $\delta=d\,\theta_{\mathrm{E}}$ and their mass ratio q. The location of the trajectory of the source relative to the lens is described by the closest angular separation $\theta_0=u_0\,\theta_{\mathrm{E}}$ between source and center of mass of the lens system and the orientation angle α relative to the line connecting the two lens components. The closest approach takes place at time t_0 and within the timespan $t_{\mathrm{E}}=\theta_{\mathrm{E}}/\mu$ the source moves by θ_{E} relative to the lens on the sky. The angular radius of the source is $\theta_{\star}=\rho_{\star}\,\theta_{\mathrm{E}}$, and as defined in Sect. 6, $F^{(s)}_{\mathrm{S}}$ and $F^{(s)}_{\mathrm{B}}$ denote the source and background fluxes, respectively.

As pointed out by Dominik (1999b), the parameters d and q are usually strongly correlated resulting in a partial parameter degeneracy which can be avoided by instead using the parameter pair (γ,q) for wide binary lenses, where γ denotes the shear and the mass ratio q measures the deviation from a Chang-Refsdal lens, or the parameter pair $(\hat{Q},q)$ for close binary lenses where $\hat{Q}$ denotes the absolute value of either eigenvalue of the traceless quadrupole moment and the mass ratio q measures the deviation from a quadrupole lens. Any (d,q) in the following text may therefore also be understood as (γ,q) or $(\hat{Q},q)$.

Rather than by the full set of $7+2n$ model parameters (d, q, u_0, α, t_0, t_{E}, $\rho_{\star}$, $F^{(s)}_{\mathrm{S}}$, $F^{(s)}_{\mathrm{B}}$), the lightcurve in the vicinity of a fold caustic is completely characterized by $3+2n$ parameters $(t^{\star}_{\mathrm{f}},t^{\perp}_{\star},F^{(s)}_{\mathrm{r}},F^{\star\,(s)}_{\mathrm{f}},\hat{\omega}^{\star}_{\mathrm{f}})$ or $2+2n$ parameters $(t^{\star}_{\mathrm{f}},t^{\perp}_{\star},F^{(s)}_{\mathrm{r}},F^{\star\,(s)}_{\mathrm{f}})$ if one disregards the parameter $\hat{\omega}^{\star}_{\mathrm{f}}$ describing the temporal variation of the magnification due to non-critical images[11], as shown in the previous section. Already a comparison of the number of parameters shows that the data over the caustic passage cannot provide an unique model for the full lightcurve of the event. Instead, they turn out to be insensitive to the caustic crossing angle ϕ and the caustic rise parameter ζ_{f}, as well as to the caustic strength R_{f} and the magnification $A^{\star}_{\mathrm{f}}$ at the beginning of the caustic entry or the end of the caustic exit, the last two parameters given by the choice of the singularity $\boldsymbol{y}_{\mathrm{f}}$ for a specific binary lens characterized by (d,q). Therefore, modelling the caustic passage data does not provide measurements of the time-scale t_{E}, the source and background fluxes $F^{(s)}_{\mathrm{S}}$ and $F^{(s)}_{\mathrm{B}}$, the source size parameter $\rho_{\star}$, and of the characteristics of the binary lens, namely the separation parameter d and the mass ratio q.

As will be discussed later in this section, there are however some relations between and restrictions on these parameters. In particular, the different rise fluxes $F^{(s)}_{\mathrm{r}}$ provide relations between the source fluxes $F^{(s)}_{\mathrm{S}}$, and together with the caustic passage fluxes $F^{\star\,(s)}_{\mathrm{f}}$ yield relations between the background fluxes $F^{(s)}_{\mathrm{B}}$, while the parameter $\hat{\omega}^{\star}_{\mathrm{f}}$ constrains the caustic crossing angle ϕ and relates it to the caustic rise parameter ζ_{f}. Moreover, additional constraints apply if measurements of properties of the full lightcurve such as the time-scale t_{E}, source, background or baseline fluxes $F^{(s)}_{\mathrm{S}}$, $F^{(s)}_{\mathrm{B}}$, or $F^{(s)}_{\mathrm{base}}$, or blend ratios $g^{(s)}$ are taken into account as discussed in Sect. 7.5.

Nevertheless, with a determination of the angular radius of the source $\theta_{\star}$, e.g. from spectral typing, the caustic passage data yield the proper motion $\mu^{\perp}$ perpendicular to the caustic with $t^{\perp}_{\star}$ as

$$\mu^{\perp}=\frac{\theta_{\star}}{t^{\perp}_{\star}}\,, \quad (77)$$

whereas the measurement of the full proper motion μ requires the determination of the caustic crossing angle ϕ

$$\mu=\frac{\theta_{\star}}{t_{\star}}=\frac{\theta_{\star}}{t^{\perp}_{\star}\,\sin\phi}\geqslant\mu^{\perp}\,, \quad (78)$$

where the caustic passage data only yield a lower limit.

As pointed out by Albrow et al. (1999b), rather than performing a parameter search on the $7+2n$-dimensional full parameter set (d, q, u_0, α, t_0, t_{E}, $\rho_{\star}$, $F^{(s)}_{\mathrm{S}}$, $F^{(s)}_{\mathrm{B}}$), all suitable binary lens models can efficiently be found by using the constraints arising from modelling the data around the caustic passage yielding the $3+2n$ parameters $(t^{\star}_{\mathrm{f}},t^{\perp}_{\star},F^{(s)}_{\mathrm{r}},F^{\star\,(s)}_{\mathrm{f}},\hat{\omega}^{\star}_{\mathrm{f}})$, so that only a 4-dimensional (or 5-dimensional if $\hat{\omega}^{\star}_{\mathrm{f}}$ is ignored) remaining parameter subspace needs to be searched for solutions. This search can be performed by creating a suitable parameter grid, and by assessing the goodness-of-fit of the arising trial models to the data. For promising regions of the parameter grid, the grid may be refined in order to succeed towards optimal models and/or the trial models can be used as initial guesses for fits in the full parameter space.

A convenient parametrization of the remaining subspace is given by $(d,q,\ell,\phi,\zeta_{\mathrm{f}})$, where the separation parameter d and the mass ratio q are the binary lens characteristics, ℓ stands for the path length along the caustic and yields the location of the fold singularity $\boldsymbol{y}_{\mathrm{f}}$, while the caustic crossing angle ϕ and the caustic rise parameter ζ_{f} characterize the source trajectory.

For a given fold singularity at $\boldsymbol{y}_{\mathrm{f}}$, the local characteristics R_{f}, $\boldsymbol{n}_{\mathrm{f}}$, A_{f} and $(\boldsymbol{\nabla}A)_{\mathrm{f}}$ are functions of derivatives of the Fermat potential of the lens mapping at the critical image $\boldsymbol{x}_{\mathrm{f}}$ or the non-critical

[11] While the inclusion of $\hat{\omega}^{\star}_{\mathrm{f}}$ as a model parameter yields more adequate estimates for other model parameters, its value itself is rather uncertain and unreliable.

images $\boldsymbol{x}^{(i)}$ which are given by Eqs. (32), (14), (45), and (50), respectively, where $\boldsymbol{n}_\mathrm{f} = \boldsymbol{e}^{(2)}$. In principle, the binary lens model yields $A_\mathrm{other}(t)$ for any source trajectory and source size. However, as pointed out in Sect. 4, within the validity of the approximation given by Eq. (64), $A_\mathrm{other}(t) = A^\mathrm{P}_\mathrm{other}(t)$ which itself is simply characterized by the coefficients $A^\star_\mathrm{f}$ and $\dot{A}^\star_\mathrm{f}$. If the value of $\hat{\omega}^\star_\mathrm{f}$ is disregarded corresponding to a constant $A^\mathrm{P}_\mathrm{other}$, one obtains $A^\star_\mathrm{f} = A_\mathrm{f}$, whereas otherwise $A^\star_\mathrm{f} = A_\mathrm{f} - \zeta_\mathrm{f}\,\hat{\omega}^\star_\mathrm{f}\,t^\perp_\star$.

7.2 Parameter search disregarding $\hat{\omega}^\star_\mathrm{f}$

Let us now investigate how the choice of $(d, q, \ell, \phi, \zeta_\mathrm{f})$ together with the $2{+}2n$ fold-caustic model parameters $(t^\star_\mathrm{f}, t^\perp_\star, F^{(s)}_\mathrm{r}, F^{\star\,(s)}_\mathrm{f})$ yields the $7 + 2n$ parameters (d, q, u_0, α, t_0, t_E, $\rho_\star$, $F^{(s)}_\mathrm{S}$, $F^{(s)}_\mathrm{B}$) which characterize the full lightcurve.

Regardless of the caustic crossing angle ϕ, the choice of ζ_f dictates the values of all source fluxes $F^{(s)}_\mathrm{S}$ and for given (d, q, ℓ) the values of the time-scale of perpendicular motion $t^\perp_\mathrm{E}$, the source size parameter $\rho_\star = \theta_\star/\theta_\mathrm{E}$, and all background fluxes $F^{(s)}_\mathrm{B}$.

Explicitly, $t^\perp_\mathrm{E}$ is determined by ζ_f and R_f as

$$t^\perp_E = \frac{\zeta_\mathrm{f}^2\,\hat{t}}{R_\mathrm{f}}\,, \tag{79}$$

while the source size parameter follows from these parameters together with $t^\perp_\star$ as

$$\rho_\star = \frac{t^\perp_\star}{t^\perp_\mathrm{E}} = \frac{R_\mathrm{f}}{\zeta_\mathrm{f}^2\,\hat{t}}\,t^\perp_\star\,. \tag{80}$$

Together with the conditions $F^{(m)}_\mathrm{S} > 0$ and $A^\star_\mathrm{f} > 1$, Eq. (67) yields the relations

$$F^{\star(s)}_\mathrm{f} - F^{(s)}_\mathrm{base} \;=\; F^{(s)}_\mathrm{S}\,(A^\star_\mathrm{f} - 1) > 0\,, \tag{81}$$

$$F^{\star(s)}_\mathrm{f} - F^{(s)}_\mathrm{B} \;=\; F^{(s)}_\mathrm{S}\,A^\star_\mathrm{f} > 0\,. \tag{82}$$

From these equations and the definition of $F^{(s)}_\mathrm{r}$, Eq. (65), the source fluxes $F^{(s)}_\mathrm{S}$ and the background fluxes $F^{(s)}_\mathrm{B}$ of all n lightcurves follow as

$$F^{(s)}_\mathrm{S} \;=\; \frac{F^{(s)}_\mathrm{r}}{\zeta_\mathrm{f}}\,, \tag{83}$$

$$F^{(s)}_\mathrm{B} \;=\; F^{\star\,(s)}_\mathrm{f} - F^{(s)}_\mathrm{r}\,\frac{A^\star_\mathrm{f}}{\zeta_\mathrm{f}}\,, \tag{84}$$

while the baseline fluxes $F^{(s)}_\mathrm{base}$ and the blend ratios $g^{(s)}$ are determined as

$$F^{(s)}_\mathrm{base} \;=\; F^{\star\,(s)}_\mathrm{f} - F^{(s)}_\mathrm{r}\,\frac{A^\star_\mathrm{f} - 1}{\zeta_\mathrm{f}}\,, \tag{85}$$

$$g^{(s)} \;=\; \zeta_\mathrm{f}\,\frac{F^{\star\,(s)}_\mathrm{f}}{F^{(s)}_\mathrm{r}} - A^\star_\mathrm{f}\,, \tag{86}$$

so that $F^{(s)}_\mathrm{S}$, $F^{(s)}_\mathrm{B}$, $F^{(s)}_\mathrm{base}$ and $g^{(s)}$ depend on no other parameters than ζ_f, $A^\star_\mathrm{f}$, and the caustic passage flux parameters $F^{(s)}_\mathrm{r}$ and $F^{\star\,(s)}_\mathrm{f}$, where $F^{(s)}_\mathrm{S}$ even depends on ζ_f and $F^{(s)}_\mathrm{r}$ only.

The choice of the caustic crossing angle ϕ determines the time $t_\star = t_\mathrm{E}\,\rho_\star$ in which the source moves by its angular radius $\theta_\star$ together with the fold-caustic model parameter $t^\perp_\star$ as

$$t_\star = \frac{t^\perp_\star}{\sin\phi} \geqslant t^\perp_\star\,. \tag{87}$$

For given (d, q, ℓ) determining $\boldsymbol{y}_\mathrm{f}$ and $\boldsymbol{n}_\mathrm{f}$, ϕ fixes the location of the source trajectory determining the parameter u_0.

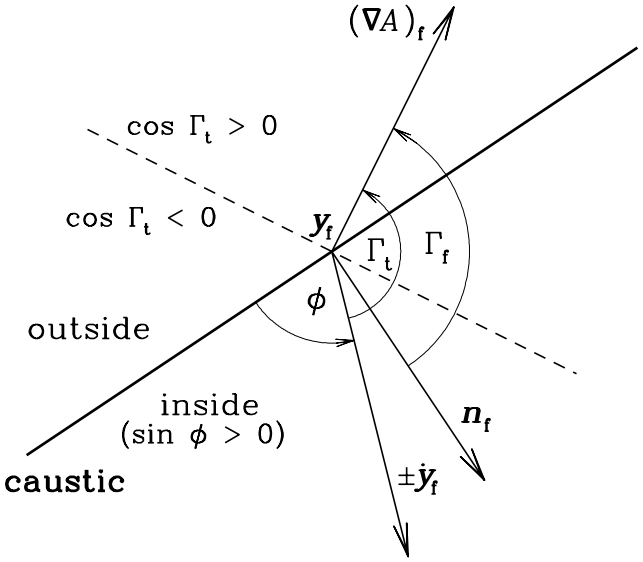

Figure 4. Definition of the angles ϕ, Γ_f, and Γ_t which describe the relative orientation between the source trajectory characterized by $\pm\,\dot{\boldsymbol{y}}_\mathrm{f}$, the caustic characterized by its inside-pointing normal $\boldsymbol{n}_\mathrm{f}$, and the gradient of the magnification $(\boldsymbol{\nabla} A)_\mathrm{f}$ of the non-critical images at the fold singularity $\boldsymbol{y}_\mathrm{f}$. Regions are marked for which the source trajectory matches the indicated conditions: $\sin\phi > 0$ ($0 < \phi < \pi$) follows from the requirement that $\pm\,\dot{\boldsymbol{y}}_\mathrm{f}$ points inside, while the condition $\zeta_\mathrm{f} > 0$ requires either $\cos\Gamma_\mathrm{t} > 0$ for $\hat{\omega}^\star_\mathrm{f} > 0$, $\cos\Gamma_\mathrm{t} < 0$ for $\hat{\omega}^\star_\mathrm{f} < 0$, or $\cos\Gamma_\mathrm{t} = 0$ for $\hat{\omega}^\star_\mathrm{f} = 0$.

The time-scale of motion $t_\mathrm{E} = t^\perp_\mathrm{E}\,\sin\phi \leqslant t^\perp_\mathrm{E}$ depends both on ζ_f and ϕ, and with R_f reads

$$t_\mathrm{E} = \frac{\zeta_\mathrm{f}^2\,\hat{t}}{R_\mathrm{f}}\,\sin\phi\,. \tag{88}$$

Finally, t_0 is determined by $t_\mathrm{f} = t^\star_\mathrm{f} \pm t^\perp_\star$, the location of the source trajectory given by $\boldsymbol{y}_\mathrm{f}$, $\boldsymbol{n}_\mathrm{f}$ and ϕ, and t_E depending on ζ_f, ϕ and R_f.

Table 1 summarizes the dependencies of the quantities characterizing the microlensing event, namely the proper motion μ and the time-scale of motion t_E as well as their transverse components $\mu^\perp$ and $t^\perp_\mathrm{E}$, the time $t_\star$ in which the sources moves by its angular radius $\theta_\star$ relative to the lens, the source size parameter $\rho_\star = \theta_\star/\theta_\mathrm{E} = t_\star/t_\mathrm{E}$, and the source and background fluxes $F^{(s)}_\mathrm{S}$ and $F^{(s)}_\mathrm{B}$, on the fold-caustic parameters $(t^\perp_\star, F^{(s)}_\mathrm{r}, F^{\star\,(s)}_\mathrm{f}, \hat{\omega}^\star_\mathrm{f})$, the parameters of the singularity $(R_\mathrm{f}, \boldsymbol{n}_\mathrm{f}, A_\mathrm{f}, (\boldsymbol{\nabla} A)_\mathrm{f})$, and the adopted caustic crossing angle ϕ and caustic rise parameter ζ_f.

7.3 Parameter search using $\hat{\omega}^\star_\mathrm{f}$

If the complete set of $3 + 2n$ fold-caustic model parameters $(t^\star_\mathrm{f}, t^\perp_\star, F^{(s)}_\mathrm{r}, F^{\star\,(s)}_\mathrm{f}, \hat{\omega}^\star_\mathrm{f})$ is used in the search of the remaining parameters required to characterize the full lightcurve, the parameter $\hat{\omega}^\star_\mathrm{f}$ provides a relation between the caustic crossing angle ϕ and the caustic rise time ζ_f, so that the parameter search is reduced to the four-dimensional subspaces (d, q, ℓ, ϕ) or $(d, q, \ell, \zeta_\mathrm{f})$.

As an alternative to expanding $A^\mathrm{P}_\mathrm{other}(t)$ which is assumed to vary slowly during the progress of the caustic passage around $t^\star_\mathrm{f}$, it may also be approximated by a linear expansion around t_f which reads

$$A^\mathrm{P}_\mathrm{other}(t) \simeq A_\mathrm{f} + (t - t_\mathrm{f})\dot{A}_\mathrm{f}\,, \tag{89}$$

where $A_\mathrm{f} = A^\mathrm{P}_\mathrm{other}(t_\mathrm{f})$ (as defined in Sect. 4) and $\dot{A}_\mathrm{f} =$

Table 1. Determination of quantities characterizing the microlensing event from the fold-caustic parameters ($t_\star^\perp$, $F_{\rm r}^{(s)}$, $F_{\rm f}^{\star\,(s)}$, $\hat\omega_{\rm f}^\star$), the parameters of the singularity ($R_{\rm f}$, $\boldsymbol{n}_{\rm f}$, $A_{\rm f}$, $(\boldsymbol{\nabla} A)_{\rm f}$), and the adopted caustic crossing angle ϕ and caustic rise parameter $\zeta_{\rm f}$.

parameter	caustic passage	singularity	crossing angle	caustic rise	other
$\mu^\perp = \frac{\theta_\star}{t_\star^\perp}$	$t_\star^\perp$				$\theta_\star$
$\mu = \frac{\theta_\star}{t_\star^\perp \sin\phi}$	$t_\star^\perp$		ϕ		$\theta_\star$
$t_\star = \frac{t_\star^\perp}{\sin\phi}$	$t_\star^\perp$		ϕ		
$\rho_\star = \frac{R_{\rm f}}{\zeta_{\rm f}^2\,\hat t}\,t_\star^\perp$	$t_\star^\perp$	$R_{\rm f}$		$\zeta_{\rm f}$	
$t_E^\perp = \frac{\zeta_{\rm f}^2\,\hat t}{R_{\rm f}}$		$R_{\rm f}$		$\zeta_{\rm f}$	
$t_{\rm E} = \frac{\zeta_{\rm f}^2\,\hat t}{R_{\rm f}}\,\sin\phi$		$R_{\rm f}$	ϕ	$\zeta_{\rm f}$	
$F_{\rm S}^{(s)} = \frac{F_{\rm r}^{(s)}}{\zeta_{\rm f}}$	$F_{\rm r}^{(s)}$			$\zeta_{\rm f}$	
$F_{\rm B}^{(s)} = F_{\rm f}^{\star\,(s)} - F_{\rm r}^{(s)}\,\frac{A_{\rm f}^\star}{\zeta_{\rm f}}$	$F_{\rm r}^{(s)}$, $F_{\rm f}^{\star\,(s)}$	$A_{\rm f}^\star$		$\zeta_{\rm f}$	

The choice of a binary lens (d, q) and of the singularity at $\boldsymbol{y}_{\rm f}$ characterized by ℓ yields $R_{\rm f}$, $\boldsymbol{n}_{\rm f}$, $A_{\rm f}$, and $(\boldsymbol{\nabla} A)_{\rm f}$. If one disregards $\hat\omega_{\rm f}^\star$, $A_{\rm f}^\star = A_{\rm f}$ and the value of $(\boldsymbol{\nabla} A)_{\rm f}$ is redundant, whereas otherwise $A_{\rm f}^\star = A_{\rm f} - \zeta_{\rm f}\,\hat\omega_{\rm f}^\star\,t_\star^\perp$ depends on $\zeta_{\rm f}$ and $\hat\omega_{\rm f}^\star$, and $\hat\omega_{\rm f}^\star$, $R_{\rm f}$, $\boldsymbol{n}_{\rm f}$ and $(\boldsymbol{\nabla} A)_{\rm f}$ constrain ϕ and provide a relation to $\zeta_{\rm f}$.

$\dot A_{\rm other}^{\rm p}(t_{\rm f})$, while the corresponding expansion of $A_{\rm other}^{\rm p}(\boldsymbol{y}(t))$ in space around $\boldsymbol{y}_{\rm f}$ reads (c.f. Eq. (44))

$$A_{\rm other}^{\rm p}(\boldsymbol{y}(t)) \simeq A_{\rm f} + (t - t_{\rm f})\,\dot{\boldsymbol{y}}_{\rm f}\cdot(\boldsymbol{\nabla} A)_{\rm f}\,. \tag{90}$$

The comparison of Eq. (89) with the expansion around $t_{\rm f}^\star$, Eq. (64), yields the relations $\dot A_{\rm f}^\star = \dot A_{\rm f}$ and $A_{\rm f}^\star = A_{\rm f} \mp \dot A_{\rm f}^\star\,t_\star^\perp$, and by comparing Eq. (90) with Eq. (89), one obtains

$$\begin{aligned}\dot A_{\rm f}^\star &= \dot{\boldsymbol{y}}_{\rm f}\cdot(\boldsymbol{\nabla} A)_{\rm f}\\ &= \pm\,|\dot{\boldsymbol{y}}_{\rm f}|\,|(\boldsymbol{\nabla} A)_{\rm f}|\,\cos\Gamma_{\rm t}\,,\end{aligned} \tag{91}$$

where $\Gamma_{\rm t}$ denotes the angle measured from $\pm\,\dot{\boldsymbol{y}}_{\rm f}$ to $(\boldsymbol{\nabla} A)_{\rm f}$. As a function of the angle $0 \leqslant \Gamma_{\rm f} < 2\pi$ measured from the caustic normal $\boldsymbol{n}_{\rm f}$ to $(\boldsymbol{\nabla} A)_{\rm f}$, which is determined by the properties of the lens mapping at $\boldsymbol{y}_{\rm f}$ alone, and the caustic crossing angle $0 < \phi < \pi$, $\Gamma_{\rm t}$ reads

$$\Gamma_{\rm t} = \Gamma_{\rm f} - \phi + \frac{\pi}{2} - 2\,\pi\,\left\lfloor \frac{\Gamma_{\rm f} - \phi}{2\,\pi} + \frac{1}{2}\right\rfloor\,, \tag{92}$$

forcing $-\frac{\pi}{2} \leqslant \Gamma_{\rm t} < \frac{3\,\pi}{2}$. With this definition, $0 < \phi < \pi$ increases with a counterclockwise rotation of $\pm\,\dot{\boldsymbol{y}}_{\rm f}$. The definition of the angles ϕ, $\Gamma_{\rm f}$, and $\Gamma_{\rm t}$ is illustrated in Fig. 4.

With $\zeta_{\rm f} > 0$ and $\dot A_{\rm f}^\star = \pm\,\zeta_{\rm f}\,\hat\omega_{\rm f}^\star$, Eq. (91) requires the sign of $\cos\Gamma_{\rm t}$ and $\hat\omega_{\rm f}^\star$ to coincide. With Eq. (92) and the condition $0 < \phi < \pi$, this results in the allowed ranges for $\Gamma_{\rm t}$ and ϕ shown in Table 2. Configurations (d, q, ℓ) for which there is no viable trajectory have to be discarded.

By inserting

$$\cos\Gamma_{\rm t} = \cos\Gamma_{\rm f}\,\sin\phi - \sin\Gamma_{\rm f}\,\cos\phi\,, \tag{93}$$

and $|\dot{\boldsymbol{y}}_{\rm f}| = 1/t_{\rm E}$ as given by Eq. (88) into Eq. (91), and using $\hat\omega_{\rm f}^\star = \pm\dot A_{\rm f}^\star/\zeta_{\rm f}$, one obtains

$$\hat\omega_{\rm f}^\star = \frac{R_{\rm f}\,|(\boldsymbol{\nabla} A)_{\rm f}|}{\zeta_{\rm f}^3\,\hat t}\,K_{\rm f}(\phi)\,, \tag{94}$$

where

$$K_{\rm f}(\phi) = \cos\Gamma_{\rm f} - \sin\Gamma_{\rm f}\,\cot\phi\,. \tag{95}$$

For $\hat\omega_{\rm f}^\star \neq 0$ and $\sin\Gamma_{\rm f} \neq 0$, this yields a relation between ϕ and $\zeta_{\rm f}$, and, according to the previous subsection also between the time-scale $t_{\rm E}$ and the source and background fluxes $F_{\rm S}^{(s)}$ and $F_{\rm B}^{(s)}$, respectively. With

$$\zeta_{\rm f,ref} = \left(\frac{R_{\rm f}\,|(\boldsymbol{\nabla} A)_{\rm f}|}{\hat\omega_{\rm f}^\star\,\hat t}\right)^{1/3}\,, \tag{96}$$

one finds explicitly

$$\zeta_{\rm f}(\phi) = \zeta_{\rm f,ref}\,\left[K_{\rm f}(\phi)\right]^{1/3} \tag{97}$$

or

$$\phi(\zeta_{\rm f}) = \frac{\pi}{2} + \arctan\frac{(\zeta_{\rm f}/\zeta_{\rm f,ref})^3 - \cos\Gamma_{\rm f}}{\sin\Gamma_{\rm f}}\,. \tag{98}$$

For $\Gamma_{\rm f} = 0$, $\zeta_{\rm f}$ adopts the value $\zeta_{\rm f,ref}$ (while $\hat\omega_{\rm f}^\star > 0$), whereas $-\zeta_{\rm f,ref}$ is adopted for $\Gamma_{\rm f} = \pi$ (while $\hat\omega_{\rm f}^\star < 0$), irrespective of ϕ. For $\hat\omega_{\rm f}^\star = 0$, one finds that $\phi = \Gamma_{\rm f}$ for $\Gamma_{\rm f} \in (0, \pi)$ or $\phi = \Gamma_{\rm f} - \pi$ for $\Gamma_{\rm f} \in (\pi, 2\pi)$. Therefore, the remaining parameter space can be parametrized by (d, q, ℓ, ϕ) for $\hat\omega_{\rm f}^\star \neq 0$ and by $(d, q, \ell, \zeta_{\rm f})$ for $\sin\Gamma_{\rm f} \neq 0$, whereas otherwise such a parametrization is not viable due to the adoption of a single fixed value.

In analogy to $\zeta_{\rm f}$, one obtains $\dot A_{\rm f}^\star = \pm\zeta_{\rm f}\hat\omega_{\rm f}^\star$ as function of the caustic crossing angle ϕ as

$$\dot A_{\rm f}^\star(\phi) = \dot A_{\rm f,ref}^\star\,\left[K_{\rm f}(\phi)\right]^{1/3}\,, \tag{99}$$

where

$$\dot A_{\rm f,ref}^\star = \pm\left(\frac{(\hat\omega_{\rm f}^\star)^2\,R_{\rm f}\,|(\boldsymbol{\nabla} A)_{\rm f}|}{\hat t}\right)^{1/3}\,. \tag{100}$$

The function $[K_{\rm f}(\phi)]^{1/3} = \zeta_{\rm f}(\phi)/\zeta_{\rm f,ref} = \dot A_{\rm f}^\star(\phi)/\dot A_{\rm f,ref}^\star$ is shown in Fig. 5 for selected angles $\Gamma_{\rm f}$. $[K_{\rm f}(\phi)]^{1/3}$ is strictly monotonic in ϕ except for $\Gamma_{\rm f} = 0$ and $\Gamma_{\rm f} = \pi$, where the constant value ±1 is adopted. With the requirement of $\zeta_{\rm f}(\phi) > 0$ and the sign of $\dot A_{\rm f}^\star(\phi)$ to match that of $\hat\omega_{\rm f}^\star$, the range of ϕ is restricted as shown in Table 2. For $\phi \to 0$ or $\phi \to \pi$, $|[K_{\rm f}(\phi)]^{1/3}|$ tends to infinity, whereas zero is approached for $\phi \to \Gamma_{\rm f}$ or $\phi \to \Gamma_{\rm f} - \pi$, respectively.

With the caustic rise parameter $\zeta_{\rm f}$ depending on the caustic crossing angle ϕ as described by Eq. (97), the time-scale of transverse motion $t_{\rm E}^\perp$ and the source size parameter $\rho_\star = t_\star^\perp/t_{\rm E}^\perp$ also become functions of ϕ which read

$$t_{\rm E}^\perp(\phi) = t_{\rm E,ref}\,\left[K_{\rm f}(\phi)\right]^{2/3} \tag{101}$$

and

Table 2. Constraints on the orientation of the source trajectory imposed by the sign of $\hat{\omega}_{\rm f}^\star$ depending on the orientation of $(\boldsymbol{\nabla} A)_{\rm f}$ with respect to the caustic.

$\hat{\omega}_{\rm f}^\star > 0$	$\Gamma_{\rm f} \in (0,\pi)$	$-\frac{\pi}{2} < \Gamma_{\rm f} - \frac{\pi}{2} < \Gamma_{\rm t} < \frac{\pi}{2}$	$0 < \Gamma_{\rm f} < \phi < \pi$
$\hat{\omega}_{\rm f}^\star > 0$	$\Gamma_{\rm f} \in (\pi,2\pi)$	$-\frac{\pi}{2} < \Gamma_{\rm t} < \Gamma_{\rm f} - \frac{3\pi}{2} < \frac{\pi}{2}$	$0 < \phi < \Gamma_{\rm f} - \pi < \pi$
$\hat{\omega}_{\rm f}^\star > 0$	$\Gamma_{\rm f} = 0$	$-\frac{\pi}{2} < \Gamma_{\rm t} < \frac{\pi}{2}$	$0 < \phi < \pi$
$\hat{\omega}_{\rm f}^\star > 0$	$\Gamma_{\rm f} = \pi$	*no viable trajectory*	
$\hat{\omega}_{\rm f}^\star < 0$	$\Gamma_{\rm f} \in (0,\pi)$	$\frac{\pi}{2} < \Gamma_{\rm t} < \Gamma_{\rm f} + \frac{\pi}{2} < \frac{3\pi}{2}$	$0 < \phi < \Gamma_{\rm f} < \pi$
$\hat{\omega}_{\rm f}^\star < 0$	$\Gamma_{\rm f} \in (\pi,2\pi)$	$\frac{\pi}{2} < \Gamma_{\rm f} - \frac{\pi}{2} < \Gamma_{\rm t} < \frac{3\pi}{2}$	$0 < \Gamma_{\rm f} - \pi < \phi < \pi$
$\hat{\omega}_{\rm f}^\star < 0$	$\Gamma_{\rm f} = 0$	*no viable trajectory*	
$\hat{\omega}_{\rm f}^\star < 0$	$\Gamma_{\rm f} = \pi$	$\frac{\pi}{2} < \Gamma_{\rm t} < \frac{3\pi}{2}$	$0 < \phi < \pi$
$\hat{\omega}_{\rm f}^\star = 0$	$\Gamma_{\rm f} \in (0,\pi)$	$\Gamma_{\rm t} = \frac{\pi}{2}$	$\phi = \Gamma_{\rm f}$
$\hat{\omega}_{\rm f}^\star = 0$	$\Gamma_{\rm f} \in (\pi,2\pi)$	$\Gamma_{\rm t} = -\frac{\pi}{2}$	$\phi = \Gamma_{\rm f} - \pi$
$\hat{\omega}_{\rm f}^\star = 0$	$\Gamma_{\rm f} = 0$ or $\Gamma_{\rm f} = \pi$	*no viable trajectory*	

The fold-caustic model parameter $\hat{\omega}_{\rm f}^\star$ characterizes the temporal variation of the magnification due to non-critical images, $0 \leqslant \Gamma_{\rm f} = \angle(\boldsymbol{n}_{\rm f}, (\boldsymbol{\nabla} A)_{\rm f}) < 2\pi$ denotes the orientation of its gradient $(\boldsymbol{\nabla} A)_{\rm f}$ relative to the caustic inside normal $\boldsymbol{n}_{\rm f}$ at the fold singularity $\boldsymbol{y}_{\rm f}$, $\Gamma_{\rm t} = \angle(\pm\dot{\boldsymbol{y}}_{\rm f}, (\boldsymbol{\nabla} A)_{\rm f})$ is the angle between the inside pointing tangent to the source trajectory $\pm\dot{\boldsymbol{y}}_{\rm f}$ and $(\boldsymbol{\nabla} A)_{\rm f}$, and ϕ denotes the caustic crossing angle.

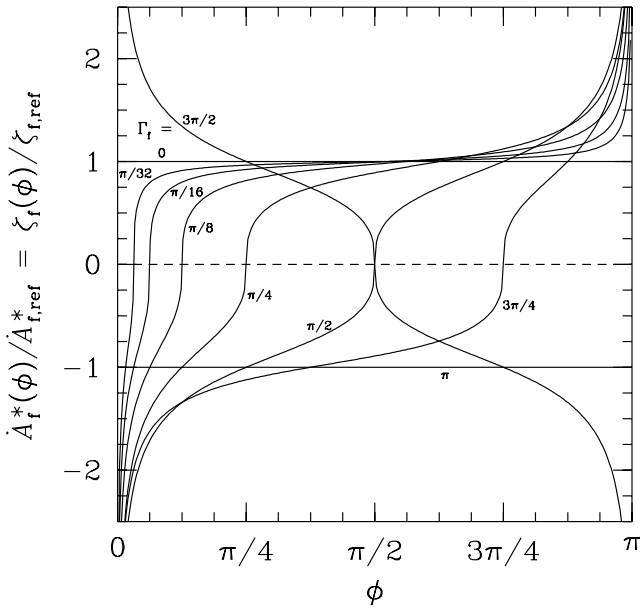

Figure 5. Variation of the magnification of the non-critical images $\dot{A}_{\rm f}^\star$ as well as the caustic rise parameter $\zeta_{\rm f}$ as a function of the caustic crossing angle ϕ for selected values of the angle $\Gamma_{\rm f}$ between caustic normal $\boldsymbol{n}_{\rm f}$ and gradient of the magnification $(\boldsymbol{\nabla} A)_{\rm f}$ of the non-critical images at the fold singularity $\boldsymbol{y}_{\rm f}$. With $\dot{A}_{\rm f,ref}^\star$ given by Eq. (100) and $\zeta_{\rm f,ref}$ given by Eq. (96), the curves show $\dot{A}_{\rm f}^\star(\phi)/\dot{A}_{\rm f,ref}^\star = \zeta_{\rm f}/\zeta_{\rm f,ref} = [K_{\rm f}(\phi)]^{1/3}$ for $\Gamma_{\rm f} =$ 0, $\pi/32$, $\pi/16$, $\pi/8$, $\pi/4$, $\pi/2$, $3\pi/4$, π, and $3\pi/2$. The range for the crossing angle ϕ is restricted as shown in Table 2, so that $\zeta_{\rm f}(\phi) > 0$ and the sign of $\dot{A}_{\rm f}^\star(\phi)$ matches that of $\hat{\omega}_{\rm f}^\star$.

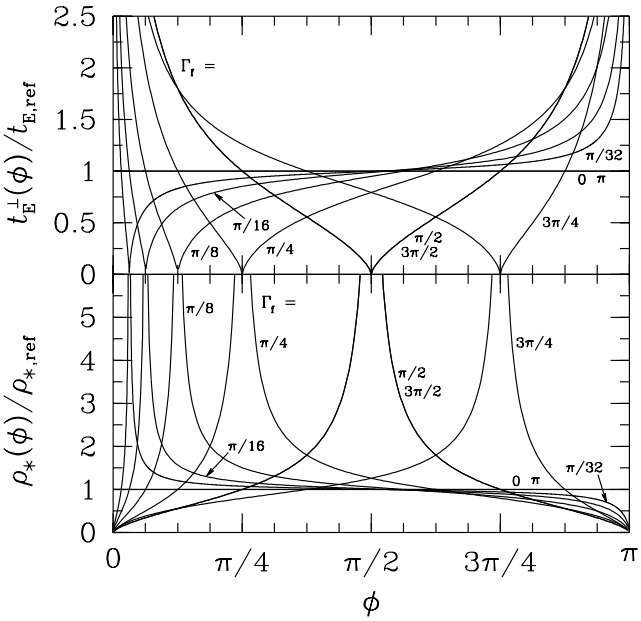

Figure 6. The dependence of the time-scale of transverse motion $t_{\rm E}^\perp$ and the source size parameter $\rho_\star = \theta_\star/\theta_{\rm E} = t_\star^\perp/t_{\rm E}^\perp$ on the caustic crossing angle ϕ. The upper panel shows curves for $t_{\rm E}^\perp(\phi)/t_{\rm E,ref} = [K_{\rm f}(\phi)]^{2/3}$ while the lower panel shows the corresponding curves for $\rho_\star(\phi)/\rho_{\star,\rm ref} = [K_{\rm f}(\phi)]^{-2/3}$ for the angle between caustic normal $\boldsymbol{n}_{\rm f}$ and gradient of the magnification of the non-critical images at the fold singularity $\boldsymbol{y}_{\rm f}$ assuming the values $\Gamma_{\rm f} =$ 0, $\pi/32$, $\pi/16$, $\pi/8$, $\pi/4$, $\pi/2$, $3\pi/4$, π, and $3\pi/2$. The reference values $t_{\rm E,ref}$ and $\rho_{\star,\rm ref}$ are given by Eqs. (103) and (104), respectively. According to the sign of $\hat{\omega}_{\rm f}^\star$, the caustic crossing angle ϕ is either restricted to the range $\Gamma_{\rm f} < \phi < \pi$ or $0 < \phi < \Gamma_{\rm f}$ for $\Gamma_{\rm f} \in (0,\pi)$ or to $\Gamma_{\rm f} - \pi < \phi < \pi$ or $0 < \phi < \Gamma_{\rm f} - \pi$ for $\Gamma_{\rm f} \in (\pi, 2\pi)$ as shown in Table 2, so that $[K_{\rm f}(\phi)]^{2/3}$ and $[K_{\rm f}(\phi)]^{-2/3}$ are strictly monotonic within the allowed range except for $\Gamma_{\rm f} = 0$ or $\Gamma_{\rm f} = \pi$, where a constant value is adopted.

$$\rho_\star(\phi) = \rho_{\star,\rm ref}\ [K_{\rm f}(\phi)]^{-2/3}\ , \tag{102}$$

respectively, where

$$t_{\rm E,ref} = R_{\rm f}^{-1/3}\ \left(\frac{|(\boldsymbol{\nabla} A)_{\rm f}|}{\hat{\omega}_{\rm f}^\star\,\hat{t}}\right)^{2/3}\ \hat{t} \tag{103}$$

and

$$\rho_{\star,\rm ref} = R_{\rm f}^{1/3}\ \left(\frac{\hat{\omega}_{\rm f}^\star\,\hat{t}}{|(\boldsymbol{\nabla} A)_{\rm f}|}\right)^{2/3}\ \frac{t_\star^\perp}{\hat{t}}\,. \tag{104}$$

For $\Gamma_{\rm f} = 0$ or $\Gamma_{\rm f} = \pi$ (i.e. $\sin\Gamma_{\rm f} = 0$), $t_{\rm E}^\perp = t_{\rm E,ref}^\perp$ and $\rho_\star = \rho_{\star,\rm ref}$ for any ϕ, whereas otherwise $t_{\rm E}^\perp(\phi)$ and $\rho_\star(\phi)$ are strictly monotonic within the allowed parameter range for ϕ shown in Table 2, where $t_{\rm E}^\perp$ reaches zero and $\rho_\star$ tends to infinity for $\phi \to \Gamma_{\rm f}$ or $\phi \to \Gamma_{\rm f} - \pi$, while $t_{\rm E}^\perp$ tends to infinity and $\rho_\star$ approaches zero for $\phi \to 0$ or $\phi \to \pi$.

The time-scale of motion $t_{\rm E}$ can also be written as function of the caustic crossing angle ϕ reading

$$t_{\rm E}(\phi) = t_{\rm E,ref}\ [K_{\rm f}(\phi)]^{2/3}\ \sin\phi\,, \tag{105}$$

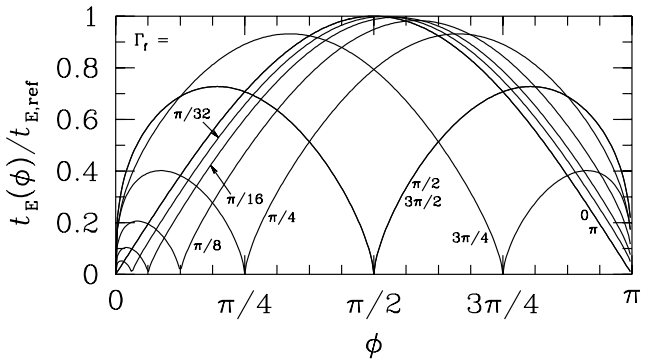

Figure 7. The time-scale of motion $t_{\rm E}$ as a function of the caustic crossing angle ϕ for different selected angles $\Gamma_{\rm f}$ between caustic normal $\boldsymbol{n}_{\rm f}$ and gradient of the magnification $(\boldsymbol{\nabla} A)_{\rm f}$ of the non-critical images at the fold singularity $\boldsymbol{y}_{\rm f}$. The curves show $t_{\rm E}(\phi)/t_{\rm E,ref} = [K_{\rm f}(\phi)]^{2/3}\,\sin\phi$, where $t_{\rm E,ref}$ is given by Eq. (103), for $\Gamma_{\rm f} = 0$, $\pi/32$, $\pi/16$, $\pi/8$, $\pi/4$, $\pi/2$, $3\pi/4$, π, and $3\pi/2$. According to Table 2, the condition $\zeta_{\rm f} > 0$ restricts ϕ either to the range $\Gamma_{\rm f} < \phi < \pi$ or $0 < \phi < \Gamma_{\rm f}$ for $\Gamma_{\rm f} \in (0, \pi)$ or to $\Gamma_{\rm f} - \pi < \phi < \pi$ or $0 < \phi < \Gamma_{\rm f} - \pi$ for $\Gamma_{\rm f} \in (\pi, 2\pi)$ depending on the sign of $\hat{\omega}_{\rm f}^\star$. Therefore, $t_{\rm E}(\phi)$ has a unique maximum within the allowed range of caustic crossing angles ϕ, whereas $t_{\rm E}(\phi)$ approaches zero at its boundaries.

with $t_{\rm E,ref}$ as defined by Eq. (103), so that $t_{\rm E}$ reaches a unique maximum within the allowed range for ϕ and approaches zero at its boundaries, located at $\phi = 0$, $\phi = \pi$, $\phi = \Gamma_{\rm f}$ or $\phi = \Gamma_{\rm f} - \pi$. Antiparallel orientations of the gradient of the magnification of the non-critical images relative to the caustic normal for which $\Gamma_{\rm f}$ differs by (an odd multiple of) π yield identical values for $t_{\rm E}^\perp$, $\rho_\star$, and $t_{\rm E}$. Fig. 6 shows $t_{\rm E}^\perp(\phi)/t_{\rm E,ref} = [K_{\rm f}(\phi)]^{2/3}$ and $\rho_\star(\phi)/\rho_{\star,{\rm ref}} = [K_{\rm f}(\phi)]^{-2/3}$ while Fig. 7 shows $t_{\rm E}(\phi)/t_{\rm E,ref} = [K_{\rm f}(\phi)]^{2/3}|\,\sin\phi$ for the same selected values of $\Gamma_{\rm f}$ as chosen for Fig. 5.

Depending on the sign of $\hat{\omega}_{\rm f}^\star$, $A_{\rm other}^{\rm p}(t)$ as given by the expansion in Eq. (64) yields unphysical values $A_{\rm other}^{\rm p}(t) \leqslant 1$ for either sufficiently large or small t. For the region containing data near the caustic passage and at least during the caustic passage itself, one should require $A_{\rm other}^{\rm p}(t) > 1$. This condition yields an upper limit for the caustic rise parameter $\zeta_{\rm f}$, which is limited to the range

$$\zeta_{\rm f} < \zeta_{\rm f,var} = \frac{A_{\rm f} - 1}{|\hat{\omega}_{\rm f}^\star|\,\tau} \tag{106}$$

where $\tau \geqslant t_\star^\perp$ denotes the timespan from $t_{\rm f}$ toward the outside of the caustic for $\hat{\omega}_{\rm f}^\star > 0$ or toward the inside of the caustic for $\hat{\omega}_{\rm f}^\star < 0$, so that the constraint arises from fulfulling $A_{\rm other}^{\rm p}(t) > 1$ at the time $t_{\rm f} - \tau$ for $\pm\,\hat{\omega}_{\rm f}^\star > 0$ and $t_{\rm f} + \tau$ for $\pm\,\hat{\omega}_{\rm f}^\star < 0$, while there is no constraint for $\hat{\omega}_{\rm f}^\star = 0$. By means of Eq. (98), the constraint on $\zeta_{\rm f}$ replaces the boundary at $\phi = 0$ or $\phi = \pi$ with $\phi_{\rm var} = \phi(\zeta_{\rm f})$, where the allowed range depends on the sign of $\hat{\omega}_{\rm f}^\star$ and the orientation of $(\boldsymbol{\nabla} A)_{\rm f}$ with respect to the caustic as shown in Table 3. For $\Gamma_{\rm f} = 0$ or $\Gamma_{\rm f} = \pi$, $\zeta_{\rm f}$ adopts the fixed value $|\zeta_{\rm f,ref}|$ irrespective of the caustic crossing angle ϕ, so that no restriction on ϕ results if $|\zeta_{\rm f,ref}| < \zeta_{\rm f,var}$, whereas otherwise the chosen configuration characterized by $(d, q, \ell, \zeta_{\rm f})$ has to be discarded.

7.4 Blending constraints

In the absence of blending, i.e. $F_{\rm B}^{(s)} = 0$ or $g^{(s)} = 0$ for all lightcurves, Eq. (70) fixes $\zeta_{\rm f}$ to

$$\zeta_{\rm f} = \frac{A_{\rm f}^\star}{g_{\rm f}^\star}\,, \tag{107}$$

where $g_{\rm f}^\star$ is a fold-caustic model parameter. If one disregards $\hat{\omega}_{\rm f}^\star$, the parameter search is reduced to the four-dimensional subspace (d, q, ℓ, ϕ). Otherwise, $A_{\rm f}^\star = A_{\rm f} - \zeta_{\rm f}\,\hat{\omega}_{\rm f}^\star\,t_\star^\perp$, so that

$$\zeta_{\rm f} = \frac{A_{\rm f}}{g_{\rm f}^\star + \hat{\omega}_{\rm f}^\star\,t_\star^\perp}\,, \tag{108}$$

and ϕ is determined by means of Eq. (98), leaving only the three-dimensional subspace (d, q, ℓ) to be explored.

Restricting the parameter space to non-negative background fluxes, i.e. $F_{\rm B}^{(s)} \geqslant 0$ or $g^{(s)} \geqslant 0$, yields a lower limit to $\zeta_{\rm f}$, limiting it to the range

$$\zeta_{\rm f} \geqslant \zeta_{\rm f,B} = \frac{A_{\rm f}}{\hat{g}_{\rm f,min}^\star + \hat{\omega}_{\rm f}^\star\,t_\star^\perp}\,, \tag{109}$$

with $g_{\rm f,min}^\star > 0$ being defined by Eq. (73). The condition $g_{\rm f,min}^\star > 0$ corresponds to the fluxes for all sites at time $t_{\rm f}^\star$ (when the leading limb of the source enters or its trailing limb exits the caustic) to fulfill $F_{\rm f}^{\star\,(s)} > 0$ for $F_{\rm B}^{(s)} \geqslant 0$, whereas at least one of the conditions $F_{\rm S}^{(s)} > 0$ and $A_{\rm f}^\star > 1$ would be violated if $F_{\rm f}^{\star\,(s)} \leqslant 0$. Similarly, the simulataneous fulfillment of $F_{\rm S}^{(s)} > 0$, $A_{\rm f} > 1$ and $F_{\rm B}^{(s)}$ implies the fluxes at time $t_{\rm f}$ (when the source center crosses the caustic) to be restricted to $F_{\rm fold}(t_{\rm f}) = F_{\rm f}^{\star\,(s)} + F_{\rm r}^{(s)}\,\hat{\omega}_{\rm f}^\star\,t_\star^\perp = F_{\rm S}^{(s)} A_{\rm f} + F_{\rm B}^{(s)} > 0$, so that $g_{\rm f,min}^\star + \hat{\omega}_{\rm f}^\star\,t_\star^\perp > 0$ needs to be fulfilled, posing a further restriction in the case $\hat{\omega}_{\rm f}^\star < 0$.

The blending limit on $\zeta_{\rm f}$ given by Eq. (109) implies a lower limit to the time-scale of perpendicular motion

$$t_{\rm E}^\perp \geqslant \frac{\zeta_{\rm f,B}^2}{R_{\rm f}}\,\hat{t}\,, \tag{110}$$

and an upper limit to the source size parameter

$$\rho_\star \leqslant \frac{R_{\rm f}}{\zeta_{\rm f,B}^2}\,\frac{t_\star^\perp}{\hat{t}}\,, \tag{111}$$

while the ranges of the fluxes and blend ratios are restricted to

$$0 \;\leqslant\; F_{\rm S}^{(s)} \;\leqslant\; F_{\rm r}^{(s)}/\zeta_{\rm f,B}\,, \tag{112}$$

$$F_{\rm B}^{(s)} \;\geqslant\; F_{\rm f}^{\star\,(s)} - F_{\rm r}^{(s)}\,g_{\rm f,min}^\star \;\geqslant\; 0\,, \tag{113}$$

$$F_{\rm base}^{(s)} \;\geqslant\; F_{\rm f}^{\star\,(s)} - F_{\rm r}^{(s)}\left(g_{\rm f,min}^\star - \frac{1}{\zeta_{\rm f,B}}\right) \;\geqslant\; F_{\rm S}^{(s)}\,, \tag{114}$$

$$g^{(s)} \;\geqslant\; \left(\frac{F_{\rm f}^{\star\,(s)}}{F_{\rm r}^{(s)}} - g_{\rm f,min}^\star\right)\zeta_{\rm f,B} \;\geqslant\; 0\,. \tag{115}$$

By definition,

$$g_{\rm f,min}^\star \leqslant \frac{F_{\rm f}^{\star\,(s)}}{F_{\rm r}^{(s)}}\,, \tag{116}$$

where the equality holds for the lightcurve $s_{\rm min}$ involving the minimal value $g_{\rm f}^{\star\,(s_{\rm min})} = g_{\rm f,min}^\star$.

With $\phi(\zeta_{\rm f})$ given by Eq. (98) if one takes the fold-caustic model parameter $\hat{\omega}_{\rm f}^\star$ into account, the lower limit on $\zeta_{\rm f}$ due to non-negative backgrounds translates into a limit $\phi(\zeta_{\rm f,B}) = \phi(\zeta_{\rm f,B})$ for the caustic crossing angle ϕ, which replaces the boundary at $\Gamma_{\rm f}$ (for $\Gamma_{\rm f} \in (0, \pi)$) or $\Gamma_{\rm f} - \pi$ (for $\Gamma_{\rm f} \in (\pi, 2\pi)$) as shown in Table 3. With $\zeta_{\rm f} = |\zeta_{\rm f,ref}|$ for $\Gamma_{\rm f} = 0$ or $\Gamma_{\rm f} = \pi$ irrespective of the caustic crossing angle ϕ, no restriction on ϕ results if $|\zeta_{\rm f,ref}| \geqslant \zeta_{\rm f,B}$, whereas the configuration $(d, q, \ell, \zeta_{\rm f})$ provides no viable solution otherwise.

Table 3. Constraints on the caustic crossing angle ϕ due to a limit on the variation of the magnification of non-critical images and the requirement of non-negative background fluxes.

$\hat{\omega}_{\rm f}^\star > 0$	$\Gamma_{\rm f} \in (0,\pi)$	$0 < \Gamma_{\rm f} < \phi_{\rm var} < \pi$	$0 < \Gamma_{\rm f} < \phi_{\rm B} < \pi$	$0 < \Gamma_{\rm f} < \phi_{\rm B} \leqslant \phi < \phi_{\rm var} < \pi$
$\hat{\omega}_{\rm f}^\star > 0$	$\Gamma_{\rm f} \in (\pi,2\pi)$	$0 < \phi_{\rm var} < \Gamma_{\rm f} - \pi < \pi$	$0 < \phi_{\rm B} < \Gamma_{\rm f} - \pi < \pi$	$0 < \phi_{\rm var} < \phi \leqslant \phi_{\rm B} < \Gamma_{\rm f} - \pi < \pi$
$\hat{\omega}_{\rm f}^\star < 0$	$\Gamma_{\rm f} \in (0,\pi)$	$0 < \phi_{\rm var} < \Gamma_{\rm f} < \pi$	$0 < \phi_{\rm B} < \Gamma_{\rm f} < \pi$	$0 < \phi_{\rm var} < \phi \leqslant \phi_{\rm B} < \Gamma_{\rm f} < \pi$
$\hat{\omega}_{\rm f}^\star < 0$	$\Gamma_{\rm f} \in (\pi,2\pi)$	$0 < \Gamma_{\rm f} - \pi < \phi_{\rm var} < \pi$	$0 < \Gamma_{\rm f} - \pi < \phi_{\rm B} < \pi$	$0 < \Gamma_{\rm f} - \pi < \phi_{\rm B} \leqslant \phi < \phi_{\rm var} < \pi$

The upper limit $\zeta_{\rm f} < \zeta_{\rm f,var}$ which avoids $A^{\rm P}_{\rm other}(t) < 1$ over the temporal range covered by observations and the lower limit $\zeta_{\rm f} \geqslant \zeta_{\rm f,B}$ which avoids negative background fluxes translate to the shown limits on the caustic crossing angle $\phi_{\rm var} = \phi(\zeta_{\rm f})$ or $\phi_{\rm B} = \phi(\zeta_{\rm f,B})$, respectively, with $\phi(\zeta_{\rm f})$ given by Eq. (98), where the allowed range depends on the temporal variation of the magnification due to the non-critical images described by the fold-caustic model parameter $\hat{\omega}_{\rm f}^\star$ and the the orientation of their gradient $(\boldsymbol{\nabla} A)_{\rm f}$ given by the angle $\Gamma_{\rm f}$ between the caustic inside normal $\boldsymbol{n}_{\rm f}$ and $(\boldsymbol{\nabla} A)_{\rm f}$. The variation limit $\phi_{\rm var}$ replaces the boundary at $\phi = 0$ or $\phi = \pi$, whereas the blending limit $\phi_{\rm B}$ replaces the boundary at $\phi = \Gamma_{\rm f}$ or $\phi = \Gamma_{\rm f} - \pi$.

7.5 Constraints from data outside the caustic-passage region

The tails of the lightcurve of a binary lens microlensing event approach those of a single lens event. From data taken in the corresponding regions (far outside the caustic passages), the baseline fluxes $F_{\rm base}^{(\rm s)}$ are easily determined while data of better quality will allow to determine the time-scale of motion $t_{\rm E}$ and the blend ratios $g^{(\rm s)}$, yielding measurements of the source fluxes $F_{\rm S}^{(s)}$ and the background fluxes $F_{\rm B}^{(s)}$. As will be pointed out later, measurements of these parameters are vital for constraining the mass ratio q and the angular separation $d\,\theta_{\rm E}$ of the binary lens and for predicting other caustic passages.

If the source flux $F_{\rm S}^{(k)}$ is known for (at least) one site k, the caustic rise parameter $\zeta_{\rm f}$ is determined as

$$\zeta_{\rm f} = \frac{F_{\rm r}^{(k)}}{F_{\rm S}^{(k)}}\,, \tag{117}$$

while it follows from the background flux $F_{\rm B}^{(k)}$, baseline flux $F_{\rm base}^{(k)}$ or blend ratio $g^{(k)}$ with $A_{\rm f}$ as

$$\zeta_{\rm f} = \frac{F_{\rm r}^{(k)}}{F_{\rm f}^{\star\,(k)} + F_{\rm r}^{(k)}\,\hat{\omega}_{\rm f}^\star\,t_\star^\perp - F_{\rm B}^{(k)}}\,A_{\rm f}\,, \tag{118}$$

$$\zeta_{\rm f} = \frac{F_{\rm r}^{(k)}}{F_{\rm f}^{\star\,(k)} + F_{\rm r}^{(k)}\,\hat{\omega}_{\rm f}^\star\,t_\star^\perp - F_{\rm base}^{(k)}}\,(A_{\rm f}-1)\,, \tag{119}$$

$$\zeta_{\rm f} = \frac{F_{\rm r}^{(k)}}{F_{\rm f}^{\star\,(k)} + F_{\rm r}^{(k)}\,\hat{\omega}_{\rm f}^\star\,t_\star^\perp}\,\left(A_{\rm f}+g^{(k)}\right)\,. \tag{120}$$

The conditions $F_{\rm S}^{(k)} > 0$ and $A_{\rm f} > 1$ imply $F_{\rm fold}(t_{\rm f}) = F_{\rm S}^{(k)} A_{\rm f} + F_{\rm B}^{(k)} = F_{\rm f}^{\star\,(k)} + F_{\rm r}^{(k)}\,\hat{\omega}_{\rm f}^\star\,t_\star^\perp > F_{\rm B}^{(k)}$ and $F_{\rm f}^{\star\,(k)} + F_{\rm r}^{(k)}\,\hat{\omega}_{\rm f}^\star t_\star^\perp > F_{\rm base}^{(k)}$, so that $\zeta_{\rm f} > 0$ is ensured. If $F_{\rm f}^{\star\,(k)} + F_{\rm r}^{(k)}\,\hat{\omega}_{\rm f}^\star = 0$, $\zeta_{\rm f}$ cannot be determined from $g^{(k)}$, whereas $A_{\rm f}$ follows directly as $A_{\rm f} = -g^{(k)}$ in this case.

The coefficient $A_{\rm f}^\star = A_{\rm f} - \zeta_{\rm f}\,\hat{\omega}_{\rm f}^\star\,t_\star^\perp$ in general depends on the fold-caustic model parameters $\hat{\omega}_{\rm f}$ and $t_\star^\perp$ and on the choice of $\zeta_{\rm f}$, while for $\hat{\omega}_{\rm f}^\star = 0$, this relation reduces to $A_{\rm f}^\star = A_{\rm f}$ and $A_{\rm f}^\star$ follows directly from the choice of (d,q,ℓ).

With the values of the caustic rise fluxes $F_{\rm r}^{(s)}$, the determination of $\zeta_{\rm f}$ fixes all source fluxes $F_{\rm S}^{(s)}$ according to Eq. (83), and together with the caustic background fluxes $F_{\rm f}^{\star\,(k)}$ and $A_{\rm f}^\star$, all background fluxes $F_{\rm B}^{(s)}$, baseline fluxes $F_{\rm base}^{(s)}$ and the blend ratios $g^{(s)}$ follow according to Eqs. (84) to (86). Therefore, a measurement of one of these quantities for a single lightcurve fixes all of these quantities for the full set of lightcurves.

The fluxes $F_{\rm r}^{(s)}$ and $F_{\rm f}^{\star\,(s)}$ obtained from modelling the data near a caustic passage contain information about the relative source fluxes and the relative blending between the different lightcurves, while their absolute values are related to $\zeta_{\rm f}$ and $A_{\rm f}^\star$. Explicitly, Eq. (65) implies that the source flux for any lightcurve s is determined by the source flux for a specific lightcurve k with $F_{\rm r}^{(s)}$ and $F_{\rm r}^{(k)}$ as

$$F_{\rm S}^{(s)} = \frac{F_{\rm r}^{(s)}}{F_{\rm r}^{(k)}}\,F_{\rm S}^{(k)}\,, \tag{121}$$

while Eqs. (81) and (82) yield the background and source fluxes for any lightcurve from the corresponding values of a specific lightcurve with $F_{\rm r}^{(s)}$, $F_{\rm r}^{(k)}$, $F_{\rm f}^{\star(s)}$, and $F_{\rm f}^{\star(k)}$ as

$$F_{\rm B}^{(s)} = F_{\rm f}^{\star(s)} - \frac{F_{\rm r}^{(s)}}{F_{\rm r}^{(k)}}\,\left(F_{\rm f}^{\star(k)} - F_{\rm B}^{(k)}\right)\,, \tag{122}$$

$$F_{\rm base}^{(s)} = F_{\rm f}^{\star(s)} - \frac{F_{\rm r}^{(s)}}{F_{\rm r}^{(k)}}\,\left(F_{\rm f}^{\star(k)} - F_{\rm base}^{(k)}\right)\,. \tag{123}$$

By means of Eqs. (117) to (120), $A_{\rm f}$ can be determined if two of the parameters $F_{\rm S}^{(k)}$, $F_{\rm B}^{(k)}$, $F_{\rm base}^{(k)}$, or $g^{(k)}$ are known for the same lightcurve, which is already the case if two of these parameters are known for any pair of different lightcurves.

Similar to the fluxes, the blend ratios $g^{(s)}$ for all sites can be deduced from the value for any site $g^{(k)}$ as

$$g^{(s)} = \frac{F_{\rm r}^{(k)}}{F_{\rm r}^{(s)}}\,\frac{F_{\rm f}^{\star(s)} + F_{\rm r}^{(s)}\,\hat{\omega}_{\rm f}^\star\,t_\star^\perp}{F_{\rm f}^{\star(k)} + F_{\rm r}^{(k)}\,\hat{\omega}_{\rm f}^\star\,t_\star^\perp}\,\left(A_{\rm f}+g^{(k)}\right) - A_{\rm f}\,, \tag{124}$$

but in contrast, this relation involves the parameter $A_{\rm f}$, so that the measurement of two different blend ratios $g^{(k)} \neq g^{(l)}$ yields not only $\zeta_{\rm f}$ as a function of $A_{\rm f}$, but also

$$\begin{aligned} A_{\rm f} = {} & \Big[F_{\rm r}^{(l)}\,(F_{\rm f}^{\star(k)} + F_{\rm r}^{(k)}\,\hat{\omega}_{\rm f}^\star\,t_\star^\perp)\,g^{(l)} - \\ & - F_{\rm r}^{(k)}\,(F_{\rm f}^{\star(l)} + F_{\rm r}^{(l)}\,\hat{\omega}_{\rm f}^\star\,t_\star^\perp)\,g^{(k)}\Big] \Big/ \\ & \Big/ \Big[F_{\rm r}^{(k)}\,(F_{\rm f}^{\star(l)} + F_{\rm r}^{(l)}\,\hat{\omega}_{\rm f}^\star\,t_\star^\perp) - \\ & - F_{\rm r}^{(l)}\,(F_{\rm f}^{\star(k)} + F_{\rm r}^{(k)}\,\hat{\omega}_{\rm f}^\star\,t_\star^\perp)\Big] \end{aligned} \tag{125}$$

itself. The condition $g^{(k)} \neq g^{(l)}$ ensures that the denominator does not vanish. For $F_{\rm f}^{\star(k)} + F_{\rm r}^{(k)}\,\hat{\omega}_{\rm f}^\star\,t_\star^\perp = 0$, Eq. (125) reveals $A_{\rm f} = -g^{(k)}$, making the measurement of $g^{(l)}$ redundant for obtaining $A_{\rm f}$ in this case.

For a given (d,q,ℓ), the determination of $\zeta_{\rm f}$ not only yields all fluxes and blend ratios, but also the source size parameter $\rho_\star$ and the time-scale of perpendicular motion $t_{\rm E}^\perp$. If $\hat{\omega}_{\rm f}^\star$ is disregarded, the parameter search reduces to the four-dimensional subspace (d,q,ℓ,ϕ). Otherwise, with a measured $\hat{\omega}_{\rm f}^\star$, $\zeta_{\rm f}$ determines ϕ

with R_f, $\boldsymbol{n}_\mathrm{f}$ and $(\boldsymbol{\nabla} A)_\mathrm{f}$, so that the proper motion μ, the time $t_\star$ in which the source moves by its angular radius, the time-scale of motion t_E, and the whole lightcurve are defined, while the search of parameters is reduced to the three-dimensional subspace (d, q, ℓ).

A configuration (d, q, ℓ) can be discarded if A_f does not match the value determined from a measurement of two fluxes or two different blend ratios or from a flux and a blend ratio.

A measurement of the time-scale of motion t_E yields a relation between the caustic crossing angle ϕ and the caustic rise parameter ζ_f, depending on R_f defined by (d, q, ℓ) and the fold-caustic model parameter t_f, thereby reducing the number of free parameters by one.

The position of another caustic passage provides a relation between t_E and ϕ which also implies a relation between ζ_f and ϕ with R_f.

Since each of the measurements of $\hat{\omega}_\mathrm{f}^\star$, t_E, and the position of another caustic passage provide a relation between ζ_f and ϕ depending on R_f, $\boldsymbol{n}_\mathrm{f}$ and $(\boldsymbol{\nabla} A)_\mathrm{f}$, and a measurement of one of the fluxes $F_\mathrm{S}^{(s)}$, $F_\mathrm{B}^{(s)}$, $F_\mathrm{base}^{(s)}$ or a blend ratio $g^{(k)}$ yields ζ_f, both ζ_f and ϕ are determined and the space of free parameters reduces to the three-dimensional space (d, q, ℓ) with two of these parameters being determined, while the determination of more than two of these parameters yields constraints for (d, q, ℓ) which characterize the binary lens model and the position of the singularity on the caustic. With the restriction of non-negative background fluxes $F_\mathrm{B}^{(s)} \geqslant 0$ and ζ_f being determined, Eq. (109) yields a limit

$$A_\mathrm{f} < \zeta_\mathrm{f} \, (g_{\mathrm{f},\min}^\star + \hat{\omega}_\mathrm{f}^\star \, t_\star^\perp) \,, \tag{126}$$

which puts a restriction on the choice of the binary lens and fold singularity parameters (d, q, ℓ) for a given caustic crossing angle ϕ.

The arising constraints for (d, q, ℓ) and the power of the prediction of other caustic passages are further discussed in the following section.

8 PREDICTIVE POWER

A dense photometric sampling of binary lens microlensing events that involve fold-caustic passages provides opportunities for resolving the stellar atmosphere of the source star yielding measurements of limb-darkening coefficients, for measuring the proper motion μ of the source relative to the lens, and for obtaining the physical properties of the lens system such as the total mass, mass ratio, semimajor axis, and orbital period. From all lens properties, only the mass ratio q and the separation parameter $d = \delta/\theta_\mathrm{E}$ are observable in the lightcurve, whereas the lens mass M and the distance D_L are convolved into the time-scale of motion t_E which however can be disentangled from an assessment of effects in the lightcurve caused by the parallactic motion. The measurement of semimajor axis and orbital period is hampered by the fact that the lightcurve depends on the instantaneous angular separation only (except for some small effects caused by orbital motion) leaving inclination and eccentricity of the binary system unconstrained, so that these quantities can only be assessed statistically.

The determination of the local properties of the lens mapping near the fold singularity parametrized as described in Sect. 6 allows to study the atmosphere of the observed source star and to obtain a lower limit on its proper motion μ relative to the caustic (i.e. relative to the lens system approximately), namely its component $\mu^\perp$ perpendicular to the caustic.

A powerful test of stellar atmosphere models requires a dense coverage of the lightcurve during the caustic passage (e.g. Rhie & Bennett 1999). In order to be able to schedule the necessary observations, including taking some high-resolution spectra which will provide a deep probe of the chemical composition of the source star by means of observable variations in associated spectral lines, caustic passages need to be predicted some time ahead. Unless the source trajectory approaches a cusp, fold-caustic passages appear in pairs, comprised of a caustic entry and a subsequent caustic exit. Caustic entries are practically unpredictable before they actually occur, so that their beginning phase can only be caught by chance and immediate action has to be taken to follow the lightcurve over the caustic entry. Since the behaviour of the lightcurve around a caustic passage depends on local properties only, the data taken during the caustic entry contains practically no information about the following caustic exit (c.f. Albrow et al. 1999b; Jaroszyński & Mao 2001). However, caustic exits can be predicted using the data on the rise to the caustic passage peak. Once such a rise has progressed, the parameters $t_\mathrm{f}^\star = t_\mathrm{f}$, $F_\mathrm{r}^{(s)}$, and $F_\mathrm{f}^{\star\,(s)}$ can be determined for a point source ($t_\star^\perp = 0$) and $\hat{\omega}_\mathrm{f}^\star = 0$. When the source reaches the region where the curvature of the lightcurve changes sign, it becomes possible to assess the source size by including $t_\star^\perp > 0$ in the fit, thereby obtaining a prediction for the end of the caustic exit at $t_\mathrm{f}^\star$ which however depends on the amount of limb darkening which might be determined from a fit to the data as well as $\hat{\omega}_\mathrm{f}^\star$ at later stages.

The data taken near the caustic passage also neither provide constraints on the mass ratio q and the angular separation parameter $d = \delta/\theta_\mathrm{E}$ which characterize the binary lens nor on the location of the fold singularity $\boldsymbol{y}_\mathrm{f}$ on the corresponding caustic described by the parameter ℓ. The parameters (d, q, ℓ) are related to the fold-caustic model parameters by means of the local properties R_f, $\boldsymbol{n}_\mathrm{f}$, A_f and $(\boldsymbol{\nabla} A)_\mathrm{f}$ which are not observables themselves but affect the lightcurve through convolutions with the source size parameter $\rho_\star$ and the source and background fluxes $F_\mathrm{S}^{(s)}$ and $F_\mathrm{B}^{(s)}$. The insensitivity to source motion parallel to the caustic leaves the caustic crossing angle ϕ undetermined. The parameters (d, q, ℓ, ϕ) fix the binary lens system, the spatial position of the source trajectory, and with $t_\mathrm{f} = t_\mathrm{f}^\star \pm t_\star^\perp$ the point of time where the source center crosses. The unknown source flux (or baseline flux) results in a free caustic rise parameter ζ_f. With the rise fluxes $F_\mathrm{r}^{(s)}$, ζ_f yields the source fluxes $F_\mathrm{S}^{(s)}$, and together with the caustic baseline fluxes $F_\mathrm{f}^{\star\,(s)}$ and $A_\mathrm{f}^\star$,[12] it yields the background fluxes $F_\mathrm{B}^{(s)}$. Together with R_f, ζ_f yields the source size parameter $\rho_\star = \theta_\star/\theta_\mathrm{E}$ and the time-scale of transverse motion $t_\mathrm{E}^\perp$, while the time-scale of motion t_E also depends on ϕ.

Since the observed caustic-passage time $t_\star^\perp$ is the product of the transverse time-scale of motion $t_\mathrm{E}^\perp = t_\mathrm{E}/(\sin\phi)$ and the source size parameter $\rho_\star$, smaller sources with smaller transverse proper motion or larger sources with larger transverse proper motion can yield the same lightcurve. Moreover, the insensitivity to the crossing angle means that the same transverse proper motion can be achieved for any angle by a corresponding choice of the full proper motion.

While the determination of the model parameters for the lightcurve near the caustic passage alone cannot yield any predictions for its remaining parts, the combination with a few simple characteristics of the data outside the caustic-passage region however provides some vital constraints.

[12] $A_\mathrm{f}^\star = A_\mathrm{f} - \zeta_\mathrm{f} \, \hat{\omega}_\mathrm{f}^\star \, t_\star^\perp$, which reduces to $A_\mathrm{f}^\star = A_\mathrm{f}$ for $\hat{\omega}_\mathrm{f} = 0$.

Restrictions of the parameters (d, q, ℓ) can arise from independent measurements of (combinations of) the local properties R_f, $\boldsymbol{n}_\mathrm{f}$, A_f or $(\boldsymbol{\nabla} A)_\mathrm{f}$. As pointed out in Sect. 7.5, measurements of one baseline flux $F_\mathrm{base}^{(k)}$ and the blend ratio $g^{(k)}$ or of two blend ratios $g^{(k)}$ and $g^{(l)}$ yield A_f,[13] while measurements of $\hat{\omega}_\mathrm{f}^\star$, one baseline flux $F_\mathrm{base}^{(k)}$, and the time-scale of motion t_E provide a relation between R_f, A_f $\boldsymbol{n}_\mathrm{f}$, and $(\boldsymbol{\nabla} A)_\mathrm{f}$.

For fixed fold-caustic parameters ($t_\star^\perp$, $F_\mathrm{r}^{(s)}$, $F_\mathrm{f}^{\star\,(s)}$, $\hat{\omega}_\mathrm{f}^\star$), the full lightcurve is defined with the choice of $(d, q, \ell, \zeta_\mathrm{f}, \phi)$, so that all of its features such as the position, duration and peak flux of other caustic passages or other types of peaks, and the time-scale of motion t_E are determined.

By requiring a match of the model lightcurve with the observed data, the determination of ζ_f and ϕ or the provision of a relation between these parameters together with limits, arising from the appropriate sign of $\dot{A}_\mathrm{f}^\star$ (that allows to fulfill $\zeta_\mathrm{f} > 0$ with the sign of $\hat{\omega}_\mathrm{f}^\star$) or the restriction to positive background fluxes, therefore yields restrictions for the choice of (d, q, ℓ). Alternatively, the restrictions on $(d, q, \ell, \zeta_\mathrm{f}, \phi)$ constrain the behaviour of the lightcurve outside the caustic-passage region, so that in particular limits on the position, duration, and peak flux of other caustic passages arise. Due to intrinsic ambiguities for binary lens models (Dominik 1999a,b), a unique solution however cannot be expected and different scenarios will be possible.

A relation between ζ_f and ϕ is provided by a measurement of $\hat{\omega}_\mathrm{f}^\star$ (which also yields an upper limit on t_E) or of t_E, and together with a measurement of a baseline flux $F_\mathrm{base}^{(k)}$, ζ_f and ϕ are determined for given (d, q, ℓ).

Determining $\hat{\omega}_\mathrm{f}^\star$ and t_E fixes ζ_f and ϕ with R_f, $\boldsymbol{n}_\mathrm{f}$, and $(\boldsymbol{\nabla} A)_\mathrm{f}$. If a baseline flux $F_\mathrm{base}^{(k)}$ is known in addition, a relation between R_f, $\boldsymbol{n}_\mathrm{f}$, A_f, and $(\boldsymbol{\nabla} A)_\mathrm{f}$ results.

The observed position of another caustic passage provides a relation between t_E and ϕ which implies a relation between ζ_f and ϕ with R_f. Combining this information with measurements of one of the parameters $\hat{\omega}_\mathrm{f}^\star$, t_E or a baseline flux $F_\mathrm{base}^{(k)}$ fixes ζ_f and ϕ, while a combination with more than one of these parameters also yields relations between R_f, $\boldsymbol{n}_\mathrm{f}$, A_f, and $(\boldsymbol{\nabla} A)_\mathrm{f}$, thereby restricting (d, q, ℓ). Other features of the additional caustic passage such as its duration, its peak flux, or the flux and rate of change of flux at the limb of the source entering or exiting the caustic, yield additional restrictions which can become quite powerful (c.f. An et al. 2002).

If ζ_f is determined, the requirement of non-negative background flux $F_\mathrm{B}^{(s)} \geqslant 0$ constrains A_f, so that the choice of (d, q, ℓ) is restricted if ϕ is determined in addition.

For a worked example, some considerations about the power of different characteristics of the photometric data outside the caustic-passage region for determining the lens properties and predicting other caustic passages have been made by Albrow et al. (1999b).

9 SUMMARY

Dense high-precision photometric sampling of microlensing lightcurves during fold-caustic passages can provide both a measurement of the proper motion μ between lens and source star and a probe of the stellar atmosphere of the source star, e.g. parametrized by limb-darkening coefficients, allowing to test existing theoretical models. Making use of the alerts supplied by the current microlensing surveys OGLE and MOA, a follow-up campaign like PLANET is capable of providing 10–15 such measurements per year on different types of galactic stars.

While the duration of the caustic passage $t_\star^\perp$ obtained from modelling the data in the caustic-passage region and of the angular size of the source $\theta_\star$, which can be obtained by spectral typing, directly yield the proper motion $\mu^\perp = \theta_\star / t_\star^\perp$ of the source perpendicular to the caustic, the full proper motion $\mu = \mu^\perp / (\sin\phi)$ only follows with a determination of the caustic crossing angle ϕ from a model of the full lightcurve.

During fold-caustic passages, the microlensing lightcurve shows an increased sensitivity to the parallactic motion of the Earth around the Sun and to the orbital motion of the binary lens whose measurement breaks the degeneracy that remains between lens mass M and distance D_L after determination of the proper motion μ (Dominik 1998; An et al. 2002). Therefore, microlensing events that involve caustic passages are prime objects for determining the mass function and the phase-space distribution of stellar populations whose constituents act as gravitational microlenses.

Moreover, the prominent feature of caustic-passage peaks allows a proper determination of binary lens parameters and with the possibility to measure μ, M and D_L individually, a reasonable opportunity is provided for obtaining statistical distributions of properties of stellar and sub-stellar binaries such as their mass, mass ratio, semimajor axis, and orbital period.

For a given distribution of lens masses, the lens mapping maps the position of an observed image of a source star to its true position. While there is a unique true source position for any observed image, a source may have several images. While the lens mapping is regular (i.e. its Jacobian determinant does not vanish), it can be locally inverted, so that the number of images only changes if the source reaches a singular point of the lens mapping. The lowest-order singularities are folds which form closed curves called critical curves in the space of image positions and caustics in the space of true source positions. When a point source crosses a fold caustic from the 'inside' to the 'outside', the magnification of two of its images diverges with the inverse square-root of the distance perpendicular to the caustic, where these two images become critical, while they disappear just as the source exits the caustic. The fold caustic is characterized by the single parameter R_f describing its strength, i.e. a proportionality factor between the magnification and the inverse square-root of the perpendicular source-caustic distance.

The magnification of the critical images of an extended source with source size parameter $\rho_\star = \theta_\star / \theta_\mathrm{E}$ is characterized by a universal caustic profile function describing the shape of the lightcurve during a caustic passage which is characteristic for any given radial brightness profile of the source, while for the same caustic strength R_f, the magnification is proportional to $\rho_\star^{-1/2}$. If the luminosity of the source at the limb does not vanish, a discontinuous change in the slope of the lightcurve is produced as the leading limb of the caustic hits the caustic. On the source further entering the caustic, the magnification rises to a peak and then drops asympotically proportional to the inverse square-root of the perpendicular distance of the source center from the caustic.

The caustic-passage regions of n observed lightcurves (for different sites and/or spectral bands) during a caustic passage can be

[13] $F_\mathrm{base}^{(k)}$ is easily obtained as observable of the lightcurve, while $g^{(k)}$ is also determined with $F_\mathrm{base}^{(k)}$ and a measurement of either the source flux $F_\mathrm{S}^{(k)}$ or the background flux $F_\mathrm{B}^{(k)}$.

characterized by the $3+2n$ parameters ($t_{\rm f}^\star$, $t_\star^\perp$, $F_{\rm r}^{(\rm s)}$, $F_{\rm f}^{\star\,(\rm s)}$, $\hat\omega_{\rm f}^\star$). The source crosses the caustic during the timespan $2\,t_\star^\perp$, where its leading limb enters or its trailing limb exits the caustic at time $t_{\rm f}^\star$ where the flux is given by $F_{\rm f}^{\star\,(\rm s)}$. $F_{\rm r}^{(\rm s)}$ denotes the flux of the two critical images at a unit time $\hat t$ after the source center enters or before it exits the caustic that are produced if the extended source is replaced by a point source at its center, and the parameter $\hat\omega_{\rm f}^\star$ measures the rate of the (constant) change of flux in units of $F_{\rm r}^{(s)}$ due to the non-critical images for the source moving inwards, while this rate is given by $-\hat\omega_{\rm f}^\star$ for a source moving outwards.

Since the influence of the lens mapping on the microlensing lightcurve near a fold-caustic can be approximated by means of local properties, the study of stellar atmospheres, and in particular the determination of limb-darkening coefficients, does not require the assessment of a complete set of model parameters that characterize the full light curve and is not influenced by ambiguities and degeneracies that are likely to occur in these parameters (Dominik & Hirshfeld 1996; Dominik 1999a,b; Albrow et al. 1999b). However, this also means that the data taken in the caustic-passage region does not provide information about the behaviour of the lightcurve outside this region. In particular, the caustic-passage data do not allow to obtain predictions about subsequent other caustic passages.

For a binary lens model and a fold singularity on its caustic, all local properties of the lens mapping can be obtained analytically by means of derivatives of the Fermat potential. However, these properties are not observables themselves but affect the lightcurve through convolutions with the source size parameter $\rho_\star$ and the source and background fluxes $F_{\rm S}^{(s)}$ and $F_{\rm B}^{(s)}$ which in general are unkown themselves. The data in the caustic-passage region therefore neither constrains the mass ratio q of the binary lens and the angular separation $\delta = d\,\theta_{\rm E}$ between its components, nor the location of the fold singularity on the corresponding caustic.

Besides parameters that characterize the source brightness profile, a microlensing event involving an extended source and a binary lens is characterized by $7+2n$ parameters. By modelling the data around an observed fold-caustic passage, thereby fixing $3+2n$ parameters, or $2+2n$ parameters if $\hat\omega_{\rm f}^\star$ is disregarded, the search for model parameters describing the full lightcurve reduces to a search in a four- or five-dimensional subspace holding the remaining parameters which can be chosen as (d,q,ℓ,ϕ) or $(d,q,\ell,\phi,\zeta_{\rm f})$, respectively, where ℓ characterizes the position of the cusp singularity on the caustic and $\zeta_{\rm f}$ characterizes the rise of the magnication on the approach to the caustic. The free choice of ϕ reflects the insensitivity to source motion parallel to the caustic, while the free choice of $\zeta_{\rm f}$ reflects the freedom in choosing the source flux. As demonstrated by Albrow et al. (1999b), this approach provides an efficient method for obtaining all suitable models that are consistent with the data of the observed microlensing event.

The determination of a few simple characteristics of the data outside the caustic-passage regions such as source, background, or baseline fluxes, the blend ratio, the time-scale of motion $t_{\rm E}$, or constraints from other characteristic observable features of the lightcurve such as the position, duration, or peak flux related to other caustic passages or other peaks yields further restrictions on the parameter space to be investigated and leads to a reduction of its dimension. This information is crucial for obtaining constraints on the mass ratio q and the angular separation parameter $d=\delta/\theta_{\rm E}$ which characterize the binary lens, and on the properties of subsequent caustic passages.

ACKNOWLEDGEMENTS

For being able to cope with the challenges arising from a long-lasting illness over more than three years, it was good to know that there are people around whose motivation in collaborating with me exceeded that of seeking the own advantage and who would sorely miss me. I would therefore like to thank those who helped me keeping well-motivated, and also for the received support on job or grant applications. In order to avoid weighting individual contributions, no names are listed here, everyone himself should be aware of his own personal involvement. Even the smallest support had a significant impact on me. I was really struck by the sudden death of one of my supporters and promise to take care that the legacy of our interaction will bear fruit.

REFERENCES

Abe F., et al., 2003, A&A, 411, L493
Afonso C., et al., 1998, A&A, 337, L17
Afonso C., et al., 2000, ApJ, 532, 340
Afonso C., et al., 2001, A&A, 378, 1014
Afonso C., et al., 2003, A&A, 404, 145
Albrow M. D., et al., 1998, ApJ, 509, 687
Albrow M. D., et al., 1999a, ApJ, 522, 1011
Albrow M. D., et al., 1999b, ApJ, 522, 1022
Albrow M. D., et al., 1999c, ApJ, 512, 672
Albrow M. D., et al., 2000, ApJ, 534, 894
Albrow M. D., et al., 2001a, ApJ, 549, 759
Albrow M. D., et al., 2001b, ApJ, 550, L173
Alcock C., et al., 1999, ApJ, 518, 44
Alcock C., et al., 2000a, ApJ, 541, 270
Alcock C., et al., 2000b, ApJ, 541, 734
Alcock C., et al., 2000c, ApJ, 542, 281
An J. H., et al., 2002, ApJ, 572, 521
Beaulieu J. P., et al., 2004, Mapping the Atmosphere of a Bulge Giant by means of Time-Resolved High-Resolution Microlensed Spectra, in preparation
Cassan A., et al., 2004, Probing the atmosphere of the bulge G5III star OGLE-2002-BUL-069 by analysis of microlensed Hα line, A&A, submitted (astro-ph/0401071)
Castro S., Pogge R. W., Rich R. M., DePoy D. L., Gould A., 2001, ApJ, 548, L197
Di Stefano R., 2000, ApJ, 541, 587
Di Stefano R., Perna R., 1997, ApJ, 488, 55
Dominik M., 1998, A&A, 329, 361
Dominik M., 1999a, A&A, 341, 943
Dominik M., 1999b, A&A, 349, 108
Dominik M., 2004a, Revealing stellar brightness profiles by means of microlensing fold caustics, MNRAS, submitted (astro-ph/0402564)
Dominik M., 2004b, Can microlensing fold caustics reveal a second stellar limb-darkening coefficient?, MNRAS, accepted (astro-ph/0403212)
Dominik M., et al., 2002, P&SS, 50, 299
Dominik M., Hirshfeld A. C., 1996, A&A, 313, 841
Fields D. L., et al., 2003, ApJ, 596, 1305
Gaudi B. S., Gould A., 1999, ApJ, 513, 619
Gaudi B. S., Petters A. O., 2002, ApJ, 580, 468
Gould A., Andronov N., 1999, ApJ, 516, 236
Gradshteyn I. S., Ryzhik I. M., 1994, Table of integrals, series and products, 5th edn. Academic Press, New York

Table 4. Used symbols

Symbol	Meaning	Definition or prime relation
Caustic-passage lightcurve		
$t_{\rm f}^\star$	time of beginning (end) of caustic entry (exit)	
$t_\star^\perp$	caustic passage half-duration	$t_\star^\perp = \rho_\star t_{\rm E}^\perp$
$\hat{\omega}_{\rm f}^\star$	temporal variation of non-critical images	$\hat{\omega}_{\rm f}^\star = \pm \dot{A}_{\rm f}^\star / \zeta_{\rm f}$
$F_{\rm r}^{(s)}$	caustic rise flux	$F_{\rm r}^{(s)} = F_{\rm S}^{(s)} \zeta_{\rm f}$
$F_{\rm f}^{\star\,(s)}$	flux at time $t_{\rm f}^\star$	$F_{\rm f}^{\star\,(s)} = F_{\rm fold}^{(s)}(t_{\rm f}^\star) = F_{\rm S}^{(s)} A_{\rm f}^\star + F_{\rm B}^{(s)}$
$g_{\rm f}^\star$	caustic rise flux ratio	$g_{\rm f}^\star = F_{\rm f}^{\star\,(s)} / F_{\rm r}^{(s)}$
$m_{\rm f}^{\star\,(s)}$	magnitude at time $t_{\rm f}^\star$	$m_{\rm f}^{\star\,(s)} = m_{\rm fold}^{(s)}(t_{\rm f}^\star)$
$\Gamma_{\{p\}}^{(s)}$	limb-darkening coefficient for profile $\propto \cos^p \vartheta$	
Caustic-passage auxiliary quantities		
$t_{\rm f}$	time when source center passes caustic	$t_{\rm f} = t_{\rm f}^\star \pm t_\star^\perp$
$\zeta_{\rm f}$	caustic rise parameter	$\zeta_{\rm f} = (t_{\rm r}/\hat{t}\,)^{1/2}$
$t_{\rm r}$	caustic rise time	$t_{\rm r} = R_{\rm f} t_{\rm E}^\perp$
Binary-lens lightcurve		
$t_{\rm E}$	event time-scale	$t_{\rm E} = \theta_{\rm E}/\mu$
u_0	lens-source impact parameter	$u_0 = \theta_0/\theta_{\rm E}$
t_0	time of closest lens-source approach	
α	angle between binary lens axis and source trajectory	
d	lens separation parameter	$d = \delta/\theta_{\rm E}$
q	binary lens mass ratio	$q = M_1/M_2$
$\rho_\star$	source size parameter	$\rho_\star = \theta_\star/\theta_{\rm E}$
$F_{\rm S}^{(s)}$	source flux	
$F_{\rm B}^{(s)}$	background flux	
$F_{\rm base}^{(s)}$	baseline flux	$F_{\rm base}^{(s)} = F_{\rm S}^{(s)} + F_{\rm B}^{(s)}$
$g^{(s)}$	blend ratio	$g^{(s)} = F_{\rm B}^{(s)} / F_{\rm S}^{(s)}$
Local lens properties		
$R_{\rm f}$	caustic strength	
$\boldsymbol{n}_{\rm f}$	caustic inside normal	
$\boldsymbol{y}_{\rm f}$	location of source singularity	$\boldsymbol{y}_{\rm f} = \boldsymbol{y}(t_{\rm f})$
$A_{\rm f}$	magnification due to non-critical images at $\boldsymbol{y}_{\rm f}$ or $t_{\rm f}$	$A_{\rm f} = A_{\rm other}^{\rm P}(\boldsymbol{y}_{\rm f}) = A_{\rm other}^{\rm P}(t_{\rm f})$
$A_{\rm f}^\star$	magnification due to non-critical images at $t_{\rm f}^\star$	$A_{\rm f}^\star = A_{\rm other}^{\rm P}(t_{\rm f}) \simeq A_{\rm f} \mp \dot{A}_{\rm f}^\star t_\star^\perp$
$\dot{A}_{\rm f}^\star$	temporal derivative of $A_{\rm other}^{\rm P}$ at $t_{\rm f}^\star$	$\dot{A}_{\rm f}^\star = \dot{A}_{\rm other}^{\rm P}(t_{\rm f}^\star) \simeq \dot{A}_{\rm other}^{\rm P}(t_{\rm f})$
$(\boldsymbol{\nabla} A)_{\rm f}$	spatial derivative of $A_{\rm other}^{\rm P}$ at $\boldsymbol{y}_{\rm f}$	$(\boldsymbol{\nabla} A)_{\rm f} = \boldsymbol{\nabla} A_{\rm other}^{\rm P}(\boldsymbol{y}_{\rm f})$
$\Gamma_{\rm f}$	angle from $\boldsymbol{n}_{\rm f}$ to $(\boldsymbol{\nabla} A)_{\rm f}$	$\Gamma_{\rm f} = \angle(\boldsymbol{n}_{\rm f}, (\boldsymbol{\nabla} A)_{\rm f})$
Lens-source motion		
ϕ	caustic crossing angle	
μ	relative lens-source proper motion	
$\mu^\perp$	lens-source proper motion perpendicular to caustic	$\mu^\perp = \mu \sin\phi$
$t_{\rm E}^\perp$	event time-scale referring to perpendicular motion	$t_{\rm E}^\perp = t_{\rm E}/(\sin\phi)$
$t_\star$	time for the source to move by its angular radius	$t_\star = \rho_\star t_{\rm E} = \theta_\star/\mu = t_\star^\perp \sin\phi$
$\dot{\boldsymbol{y}}_{\rm f}$	source proper motion vector per $\theta_{\rm E}$ at $t_{\rm f}$	$\dot{\boldsymbol{y}}_{\rm f} = \dot{\boldsymbol{y}}(t_{\rm f})$, $\lvert\dot{\boldsymbol{y}}_{\rm f}\rvert = 1/t_{\rm E}$
$\Gamma_{\rm t}$	angle from $\pm\dot{\boldsymbol{y}}_{\rm f}$ to $(\boldsymbol{\nabla} A)_{\rm f}$	$\Gamma_{\rm t} = \angle(\pm\dot{\boldsymbol{y}}_{\rm f}, (\boldsymbol{\nabla} A)_{\rm f})$
Other quantities		
$\hat{t}$	arbitrary unit time	
M	total lens mass	$M = \sum M_i$
M_i	individual lens masses	
$D_{\rm L}$	lens distance	
$D_{\rm S}$	source distance	
$\theta_\star$	angular source radius	
δ	angular separation betwen lens objects	
θ_0	smallest angular lens-source separation	
$\theta_{\rm E}$	angular Einstein radius	$\theta_{\rm E} = [(4GM/c^2)(D_{\rm S} - D_{\rm L})/(D_{\rm S} D_{\rm L})]^{1/2}$

Upper (lower) signs correspond to a caustic entry (exit), $F_{\rm fold}^{(s)}(t)$ denotes the flux, $m_{\rm fold}^{(s)}(t)$ the magnitude, $A_{\rm other}^{\rm P}(t)$ the magnification due to non-critical images, and $\boldsymbol{y}(t) = \boldsymbol{\theta}(t)/\theta_{\rm E}$ the source position as a function of time, where $\boldsymbol{\theta}(t)$ is the angular position of the source. Among the superscripts and subscripts, $\square_{\rm f}$ denotes a relation to the fold singularity, $\square^\star$ denotes a reference to the stellar limb, $\square_\star$ denotes a relation to stellar radius, $\square^\perp$ denotes the vector component perpendicular to the fold caustic, and $\square^{(s)}$ refers to a specific site and filter.

Hardy S. J., Walker M. A., 1995, MNRAS, 276, L79
Jaroszyński M., Mao S., 2001, MNRAS, 325, 1546
Mao S., Di Stefano R., 1995, ApJ, 440, 22
Mao S., Paczynski B., 1996, ApJ, 473, 57
Rhie S. H., Bennett D. P., 1999, Line Caustic Microlensing and Limb Darkening, preprint (astro-ph/9912050)
Rhie S. H., et al., 1999, ApJ, 522, 1037
Schneider P., 1985, A&A, 143, 413
Schneider P., Ehlers J., Falco E. E., 1992, Gravitational Lenses. Springer, Berlin
Schneider P., Wagoner R. V., 1987, ApJ, 314, 154
Schneider P., Weiß A., 1986, A&A, 164, 237
Schneider P., Weiß A., 1987, A&A, 171, 49
Schneider P., Weiß A., 1992, A&A, 260, 1
Sumi T., et al., 2003, ApJ, 591, 204
Udalski A., et al., 1998, Acta Astronomica, 48, 431
Udalski A., Kubiak M., Szymański M., 1997, Acta Astronomica, 47, 319
Witt H. J., Mao S., 1995, ApJ, 447, L105
Wozniak P. R., et al., 2001, Acta Astronomica, 51, 175
Yoo J., et al., 2004, ApJ, 603, 139